



HAL
open science

Monocationic Bis-Alkyl and Bis-Allyl Yttrium Complexes: Synthesis, ^{89}Y NMR Characterization, Ethylene or Isoprene Polymerization, and Modeling

Alexis D. Oswald, Aymane El Bouhali, Emmanuel Chefdeville, Pierre-Alain Breuil, H el ene Olivier-Bourbigou, Julien Thuilliez, Florent Vaultier, Aimery de Mallmann, Mostafa Taoufik, Lionel Perrin, et al.

► To cite this version:

Alexis D. Oswald, Aymane El Bouhali, Emmanuel Chefdeville, Pierre-Alain Breuil, H el ene Olivier-Bourbigou, et al.. Monocationic Bis-Alkyl and Bis-Allyl Yttrium Complexes: Synthesis, ^{89}Y NMR Characterization, Ethylene or Isoprene Polymerization, and Modeling. *Organometallics*, 2021, 40 (2), pp.218-230. 10.1021/acs.organomet.0c00709 . hal-03179735

HAL Id: hal-03179735

<https://ifp.hal.science/hal-03179735>

Submitted on 24 Mar 2021

HAL is a multi-disciplinary open access archive for the deposit and dissemination of scientific research documents, whether they are published or not. The documents may come from teaching and research institutions in France or abroad, or from public or private research centers.

L'archive ouverte pluridisciplinaire **HAL**, est destin ee au d ep ot et  a la diffusion de documents scientifiques de niveau recherche, publi es ou non,  emanant des  tablissements d'enseignement et de recherche franais ou  trangers, des laboratoires publics ou priv es.

Monocationic bis-alkyl and bis-allyl yttrium complexes, synthesis, ^{89}Y NMR characterization, ethylene or isoprene polymerization and modelling

*Alexis D. Oswald,^a Aymane El Bouhali,^b Emmanuel Chefdeville,^b Pierre-Alain R. Breuil,^c H el ene
Olivier-Bourbigou,^c Julien Thuilliez,^d Florent Vaultier,^d Aimery De Mallmann,^a Mostafa
Taoufik,^{a,*} Lionel Perrin^{b,*} and Christophe Boisson^{a,*}*

^a Univ Lyon, Universit e Claude Bernard Lyon 1, CPE Lyon, CNRS, UMR 5265, Chemistry,
Catalysis, Polymers and Processes (C2P2), 43 Bd du 11 Novembre 1918, 69616 Villeurbanne,
France

^b Univ Lyon, Universit e Claude Bernard Lyon I, CNRS, INSA, CPE, UMR 5246, ICBMS, 1 rue
Victor Grignard, F-69622 Villeurbanne cedex, France

^c IFP Energies nouvelles, Rond-point de l' changeur de Solaize, BP 3, 69360 Solaize, France

^d Manufacture Michelin, 23 places Carmes D chaux, F-63000 Clermont-Ferrand, France

yttrium • cationic complexes • synthesis • characterization • ^{89}Y NMR • ethylene • isoprene •
polymerization • DFT

ABSTRACT Monocationic complexes of yttrium with various bis-alkyl and bis-allyl ligands $Y(CH_2SiMe_2Ph)_2(THF)_4[B(C_6F_5)_4]$, $[Y(CH_2C_6H_4NMe_2)_2(THF)_2][B(C_6F_5)_4]$ and $[Y[1,3-(SiMe_3)_2C_3H_3]_2(THF)_2][B(C_6F_5)_4]$ have been prepared by protonolysis of the corresponding homoleptic tris-alkyl or -allyl complexes using the anilinium borate salt $[PhNMe_2H][B(C_6F_5)_4]$. The resulting ion-pair complexes have been isolated and characterized by different techniques such as elemental analysis, (1H , ^{13}C , ^{89}Y) NMR and EXAFS for the allyl cationic complex, $[Y[1,3-(SiMe_3)_2C_3H_3]_2(THF)_2][B(C_6F_5)_4]$. More specifically, a 1H coupled ^{89}Y INEPT sequence has been developed in order to quantify the metal / alkyl ligand stoichiometry of both synthesized neutral tris-alkyl and cationic bis-alkyl yttrium complexes. The activity of the cationic complexes towards ethylene and isoprene homopolymerization has been assessed. In presence of TiBA, polyethylene was produced with activities ranging from 6 to 26 $kgPE mol_Y^{-1} h^{-1} bar^{-1}$. The molar mass of the yielded polymers shows a bimodal distribution. Using similar conditions, polyisoprene was produced up to full conversion of the monomer. The microstructure of the yielded polyisoprene displays mainly *cis*-1,4 units (ca. 60 to 70%) and 3,4 units (ca. 20 to 30%). Only few percent of *trans*-1,4 units were revealed.

INTRODUCTION

Since the first synthesis of homoleptic alkyl rare earth complexes by Lappert et al. in 1973,^{1,2} numerous tris-alkyl or tris-allyl rare-earth complexes have been characterized and isolated.³ These complexes are used as precursors for the preparation of mono- and di-cationic alkyl or allyl molecular complexes via protonolysis-based ligand exchange reactions (see for example ref⁴). In the aim of exploring the structure and activity of new electrophilic organometallic complexes,^{5,6}

the synthesis of cationic bis-alkyl or bis-allyl rare-earth complexes was initially exemplified in 2003.^{7,8} Cationic complexes are usually prepared by reacting neutral tris-alkyl or tris-allyl complexes with a borate salt such as trityl borate $[\text{CPh}_3][\text{B}(\text{C}_6\text{X}_5)_4]$ or anilinium borate $[\text{PhNMe}_2\text{H}][\text{B}(\text{C}_6\text{X}_5)_4]$ ($\text{X} = \text{H}$ or F). Among these families of cationic complexes, cations associated to $[\text{BPh}_4]^-$ as a counter-ion (see for additional examples refs^{4,9,10,11,12,13,14,15,16}) are preferred as they do not initiate THF polymerization. The synthesis and characterization of cationic complexes associated to $[\text{B}(\text{C}_6\text{F}_5)_4]^-$ as a counter-anion (see for additional examples refs^{17,18}) appears more challenging due to their lower stability in solution and poor ability to crystallize. This could explain why, to our knowledge, only three homoleptic bis-allyl cationic complexes were isolated with $[\text{B}(\text{C}_6\text{F}_5)_4]^-$ as a counter-anion: $[\text{M}(\text{C}_3\text{H}_5)_2(\text{THF})_3][\text{B}(\text{C}_6\text{F}_5)_4]$; $\text{M} = \text{Y}, \text{La}, \text{Nd}$.¹⁹

Among rare earth elements, yttrium is of specific interest aside its availability and relatively low cost; it is one of the few rare earth elements to have a common nuclear spin I of $-1/2$ for the ^{89}Y nucleus which is of 100 % natural abundance. Additionally, with a shift range of more than 1300 ppm and a high sensitivity to the coordination sphere around the metal, ^{89}Y NMR appears as a powerful tool to characterize yttrium complexes and to monitor the structural changes induced by cationization. These characteristics were exploited in order to develop specific ^{89}Y NMR sequences to finely characterize both neutral and cationic complexes. It is worth mentioning that ^{89}Y NMR analyses are classically long lasting due to a t_1 relaxation time that is typically of the order of 60 s and a low receptivity that is roughly 0.66 that of ^{13}C . This is probably at the origin of the limited number of reported studies in which this technique is used, though assignment of ^{89}Y chemical shifts by DFT calculations is suggested to adequately complement experimental investigations.²⁰

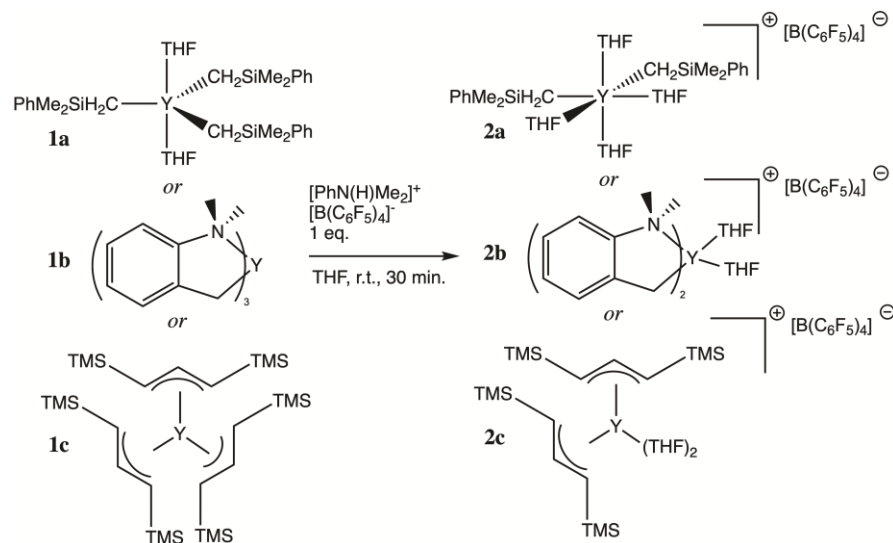
Generally, cationization of neutral bis- or tris-alkyl/allyl rare earth complexes is performed *in situ* in order to prepare cationic catalysts active towards ethylene or 1,3-diene polymerization though only few cationic rare earth complexes have been directly used for 1,3-diene polymerization.^{19,21,22}

In order to gain in structure-activity relationship and mechanism understanding, the isolation of proposed cationic species formed during the activation process is thus of high interest. In this communication paper, we report the synthesis of three original cationic bis-alkyl/allyl yttrium complexes. These yttrium complexes have been characterized by ⁸⁹Y NMR. ⁸⁹Y INEPT and proton-coupled INEPT ⁸⁹Y sequences have been developed as rapid and valuable method for characterization of yttrium complexes. These new cationic complexes have been used as catalyst precursors for ethylene and isoprene polymerization. Due to its poor ability to crystallize, the characterization of bis-allyl cationic complex has been also extended by EXAFS study at Y K-edge.

RESULTS AND DISCUSSION

Synthesis and characterizations of yttrium cationic complexes. Neutral complexes Y(CH₂SiMe₂Ph)₃(THF)₂ **1a**,²³ Y(CH₂C₆H₄NMe₂)₃ **1b**,²⁴ and Y[1,3-(SiMe₃)₂C₃H₃]₃ **1c**,²⁰ were synthesized as described in the literature. The synthesis of cationic complexes **2a**, **2b** and **2c** was performed in THF as described in [Scheme 1](#). Complexes **2a** and **2b** are rare examples of isolated cationic complexes with [B(C₆F₅)₄]⁻ as counter-anion. They have been characterized by elemental analysis and ¹H, ¹³C, ¹¹B, ¹⁹F and ⁸⁹Y NMR. As mentioned above, the monoisotopic ⁸⁹Y nucleus which has an abundance of 100% and nuclear spin I of -1/2 couples with other NMR sensitive

atoms. This property has been fruitfully derived to characterize the synthesized monocationic complexes.



Scheme 1. Synthesis of monocationic bis-alkyl and -allyl yttrium complexes. TMS = SiMe₃.

For complex **2a**, the ¹H NMR spectrum displays a doublet at -0.45 ppm with a J_{YH} coupling constant of 3 Hz characteristic of the coupling between yttrium and the methylenic protons of the -CH₂SiMe₂Ph ligand. This coupling with yttrium is also confirmed by the ¹³C-¹H NMR spectrum that displays a doublet at 32.0 ppm. The J_{YC} coupling constant has been measured to 42 Hz and is characteristic of the coupling between yttrium and the α carbon of the -CH₂SiMe₂Ph ligand. For complex **2b**, the coupling of yttrium with the protons of the methylene of the -CH₂C₆H₄NMe₂ ligand cannot be identified in the ¹H NMR spectrum due to the overlap with THF signals. However, the ¹³C NMR spectrum displays a doublet at 48.3 ppm for which the J_{YC} coupling constant is measured to 25 Hz. These complexes have been subject to further characterization by ⁸⁹Y NMR spectroscopy, and more precisely by the ¹H-⁸⁹Y HMBC experiment

(Figure S21). For complex **2b**, this NMR experiment highlights couplings between yttrium and both methylene bound to Y and methyl protons of the NMe₂ group though no doublet is apparent for the NMe₂ in the ¹H NMR spectrum (Figure S18).

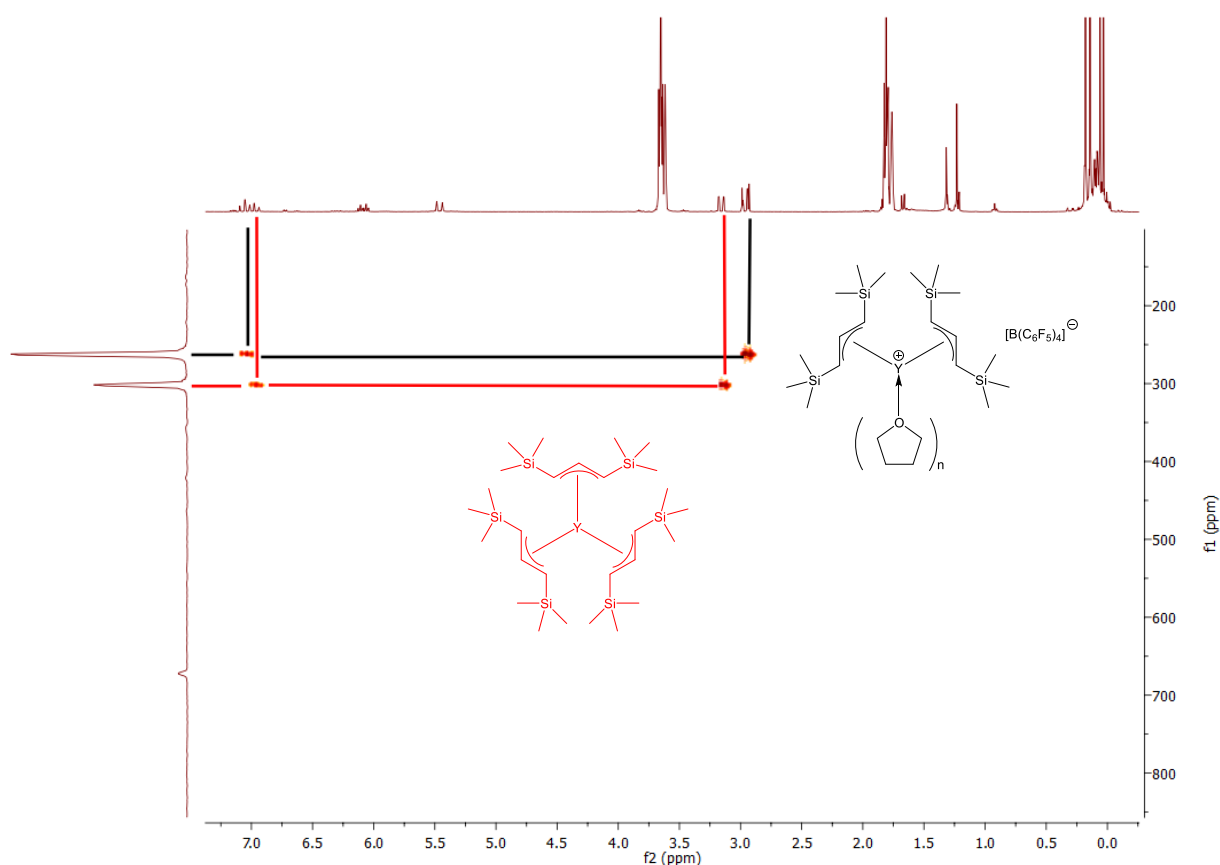


Figure 1. ¹H-⁸⁹Y HMBC NMR of [Y[1,3-(SiMe₃)₂C₃H₃]₂(THF)₂][B(C₆F₅)₄] **2c** (black) in THF-*d*₈ at 298 K in equilibria with Y[1,3-(SiMe₃)₂C₃H₃]₃ **1c** (red).

The cationization of the homoleptic tris-allyl complex **1c** yielded the cationic complex **2c** which has been also characterized by NMR spectroscopy though this complex is not stable at room temperature. ¹H NMR analysis shows a triplet of doublets of at 7.05 ppm corresponding to the proton Me₃SiCHCHHSiMe₃ of the allyl ligand. A coupling constant J_{YH} of 1.5 Hz is measured.

Nevertheless, after several hours in solution at room temperature the spectrum features the appearance of characteristic signals of the neutral species revealing the low stability of the cationic species in these conditions. As indicated in [Figure 1](#), the ^{89}Y - ^1H HMBC NMR spectrum reveals the presence of both the neutral precursor **1c** and its corresponding cation **2c**. No other product is detected by NMR though the formation of insoluble dicationic derivatives could be assumed.

Only few examples of ^{89}Y NMR spectroscopy have been reported in the literature due to the long relaxation times (t_1) of more than 60s and a low receptivity, as mentioned in the introduction. In order to take advantage of this technique for characterization of yttrium complexes, the resolvable $^2J_{\text{YH}}$ coupling was efficiently exploited via Inensitive Nuclei Enhanced by Polarization Transfer (INEPT) experiment. Interestingly, the ^{89}Y INEPT sequence greatly enhances the sensitivity and thus raises the data accumulation rate. Regarding the tris-alkyl complex **1a**, the transfer of nuclear spin polarization from ^1H to ^{89}Y enabled to reduce analysis time from 24 hours to 30 minutes ([Figure S3 and S4](#)).

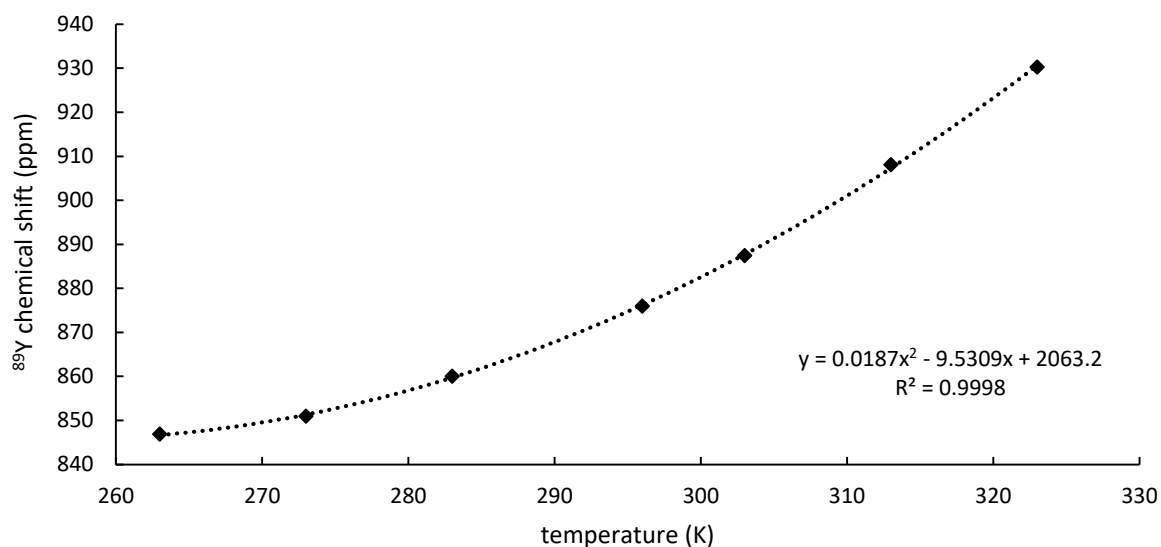


Figure 2. ^{89}Y chemical shift of $\text{Y}(\text{CH}_2\text{SiMe}_2\text{Ph})_3(\text{THF})_2$ (**1a**) in $\text{THF-}d_8$ as a function of the temperature.

Thanks to the reduced time of analysis, the influence of temperature on the ^{89}Y chemical shift can be studied. As displayed in Figure 2, temperature has a significant influence on the chemical shift: a temperature increase of 27 K induces a downfield shift of 54 ppm (876 ppm at 296 K vs. 930 ppm 323K). This temperature dependence of the yttrium chemical shift has been fitted by a second-order polynomial function as shown in Figure 2. This phenomenon may originate from the fluctuation of the dynamics of the complex **1a**²⁵ that is partly related to the variation of the density of the solvent.²⁶

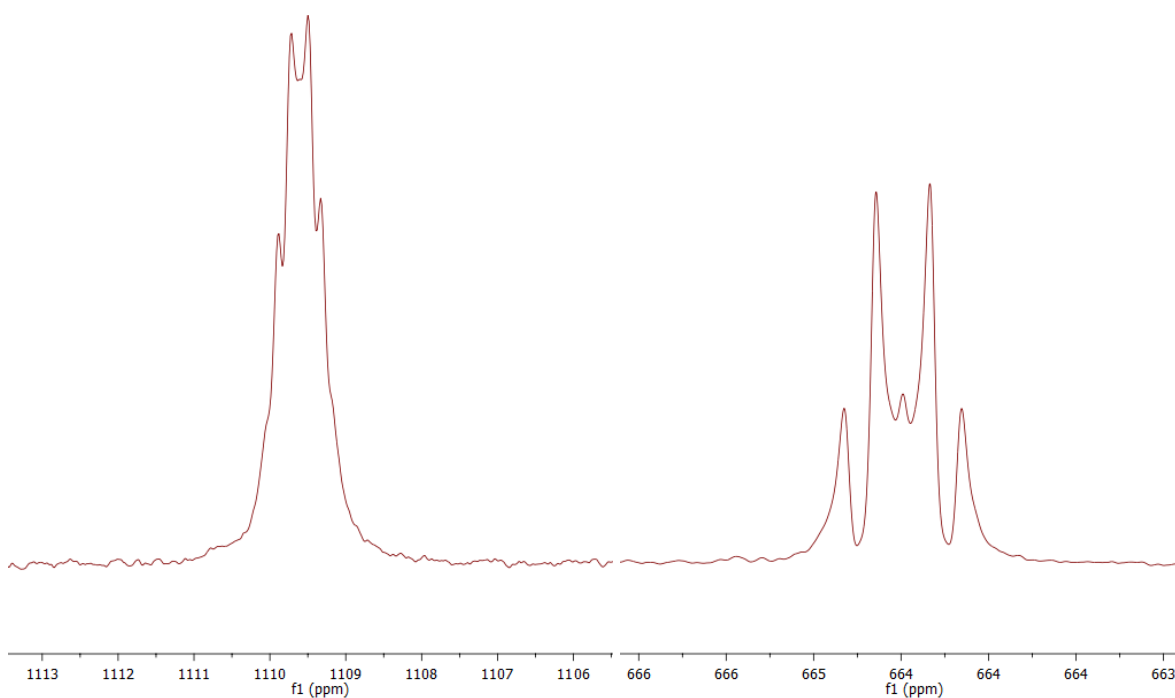


Figure 3. ^1H coupled ^{89}Y INEPT spectrum of complex $\text{Y}(\text{CH}_2\text{SiMe}_2\text{Ph})_3(\text{THF})_2$ in C_6D_6 at 298 K (left) and $[\text{Y}(\text{CH}_2\text{SiMe}_2\text{Ph})_2(\text{THF})_4][\text{B}(\text{C}_6\text{F}_5)_4]$ in $\text{THF}-d_8$ at 298 K (right).

The multiplicity of the ^{89}Y signal determined by the ^1H coupled ^{89}Y INEPT experiment enables to attribute the number of ligands coordinated to the metal center in homoleptic neutral and cationic

complexes. It is worth mentioning that a consequence of INEPT NMR sequence is the reduced intensity displayed by the central peak of the signal. Concerning the tris-alkyl complex **1a**, the spectrum of the ^1H coupled ^{89}Y INEPT experiment displays a heptuplet as shown in [Figure 3](#). This signal results thus from the coupling with six protons and agrees with the coordination of three $\text{CH}_2\text{SiMe}_2\text{Ph}$ ligands. The quintet observed for complex **2a** confirms the loss of alkyl ligand and thus supports the efficiency of the cationization reaction ([Figure 3](#)) leading to the cationic complex $[\text{Y}(\text{CH}_2\text{SiMe}_2\text{Ph})_2(\text{THF})_4][\text{B}(\text{C}_6\text{F}_5)_4]$.

Table 1. Solvent dependence of ^{89}Y NMR chemical shifts at 298 K of yttrium complexes.

run	complex	solvent	^{89}Y Chemical shift (ppm)
1	1a	C_6D_6	1109.6
2	1a	$\text{THF-}d_8$	879.5
3	2a	$\text{THF-}d_8$	664.5
4	1b	C_6D_6	389.5
5	1b	$\text{THF-}d_8$	408.5
6	2b	$\text{THF-}d_8$	434.4 ^a
7	1c	C_6D_6	480.7
8	1c	$\text{THF-}d_8$	302.9
9	2c	$\text{THF-}d_8$	263.7

^aDetermined by 2D $^1\text{H-}^{89}\text{Y}$ HMBC experiment, 440.4 ppm was measured via the ^{89}Y INEPT sequence at 328K.

Finally, we showed that the solvent has a significant influence on ^{89}Y chemical shifts of complexes **1a-c**, as shown in [Table 1](#). This may originate from the coordination of a THF molecule to the metal. As well, for cationic complexes, an important chemical shift between 26 ppm and

215 ppm could be observed depending on the analysis solvent. This point is addressed by molecular modeling in the following section.

^{89}Y NMR Modelling. White and Hanusa have reported a computational strategy that enables the prediction of ^{89}Y chemical shifts for a large set of organometallic complexes. This strategy relies on GIAO calculations performed using the O3LYP density functional on geometries preliminarily optimized at the B3PW91 level.²⁰ As we have faced issues using this specific approach, we have considered an alternative combination of density functional and basis sets. Accordingly, to the procedure previously reported by White and Hanusa,²⁰ a set of 14 Y-based complexes (Table 2, column 1) that shows a large diversity in terms of charges, coordination numbers and type of ligands has been selected and optimized at the B3PW91 level.^{27,28}

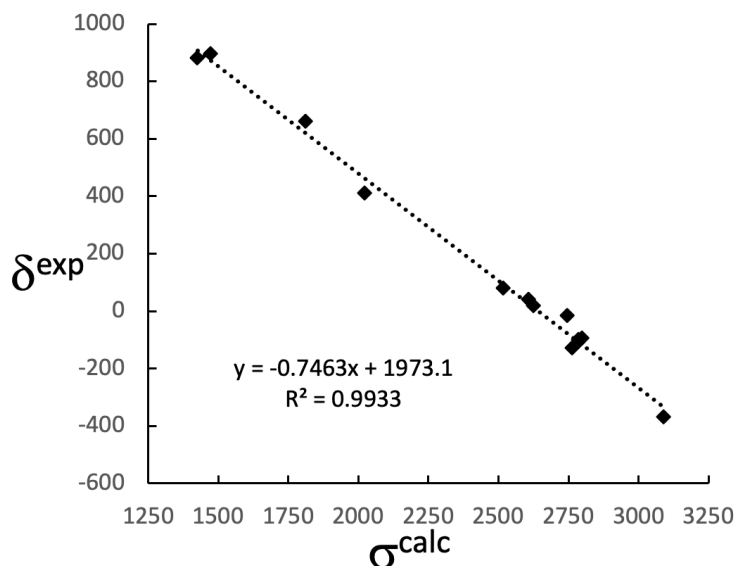


Figure 4. Plot of calculated ^{89}Y shielding against experimental ^{89}Y chemical shift of Yttrium complexes.

In these calculations, non-metal elements have been represented by all electrons polarized triple- ζ 6-311G(*d,p*) basis sets,³¹ and Y by a Godbout DGDZVP (18s12p9d)/[6s5p3d] basis set.³² Then

GIAO NMR calculations have been performed using the B3LYP density functional.^{27,33} Non-metal elements have been represented by all electrons 6-311+G(3df,3pd) basis set basis sets,^{34,35,36} and Y by an all-electrons *x2c*-TVZPall-2*c* basis set.³⁷ This level of calculation offers a good fit of the experimental chemical shifts (δ^{exp}) vs computed shielding constants (σ^{calc}) as indicated in [Table 2](#) and [Figure 4](#).

Table 2. Simulated and experimental ⁸⁹Y NMR chemical shifts of a set of yttrium complexes.

complex	experimental shift ^a	calculated shift ^a		exp. vs calc. difference	
	δ^{exp} (solvent) (ppm)	δ^b (ppm)	δ^c (ppm)	$\Delta\delta^d$ (ppm)	$\Delta\delta^e$ (ppm)
Y(C ₅ H ₄ Me) ₃ (THF) 3	-371 (THF- <i>d</i> ₈)	-339.3	-352.8	31.7	18.2
Y(C ₅ Me ₅) ₂ (OPh) 7	-129 (C ₆ D ₆)	-91.4	-85.2	37.9	44.1
Y(C ₅ H ₄ Me) ₂ Cl(THF) 1	-103 (THF- <i>d</i> ₈)	-108.2	-118.4	-5.2	-15.4
[Y(C ₅ H ₄ Me) ₂ (μ -Cl)] ₂ 4	-97 (tol- <i>d</i> ₈)	-108.3	-123.8	-11.3	-26.8
[Y(C ₅ H ₄ Me) ₂ (μ -H)(THF)] ₂ 6	-92 (THF- <i>d</i> ₈)	-118.8	-89.5	-26.8	2.5
[Y(C ₅ H ₄ Me) ₂ (μ -Me)] ₂ 5	-15 (tol- <i>d</i> ₈)	-48.5	-81	-33.5	-66.0
Y(C ₅ Me ₅)(OPh) ₂ 8	21 (C ₆ D ₆)	11.5	42.7	-9.5	21.7
Y(C ₅ H ₄ Me) ₂ (Me)(THF) 2	40 (THF- <i>d</i> ₈)	22.0	8.4	-18.0	-31.6
Y(C ₅ Me ₅) ₂ {CH(SiMe ₃) ₂ } 9	79 (C ₆ D ₆)	92.9	24.1	14.0	-54.8
[Y(CH ₂ SiMe ₃)(THF) ₄] ²⁺ 13	409 (THF- <i>d</i> ₈)	463.8	463.1	54.6	53.9
[Y(CH ₂ SiMe ₃) ₂ (THF) ₄] ⁺ 12	662 (THF- <i>d</i> ₈)	621.4	605.6	-40.8	-56.6
Y(CH ₂ SiMe ₃) ₃ (THF) ₂ 11	883 (THF- <i>d</i> ₈)	908.9	881.9	26.2	-1.1
Y(CH ₂ SiMe ₃) ₃ (THF) ₃ 14	883 (THF- <i>d</i> ₈)	758.9	757.7	-123.8 ^f	-125 ^f
Y[CH(SiMe ₃) ₂] ₃ 10	895 (tol- <i>d</i> ₈)	875.6	905	-19.4	10.0

^aExtracted from references[[29](#), [30](#), [5](#)]; ^bCalculated by our methodology; ^cReported by White and Hanusa[[20](#)]; ^d $\Delta\delta = \delta^b - \delta^{\text{exp}}$; ^e $\Delta\delta = \delta^c - \delta^{\text{exp}}$; ^fExcluded for the fit.

The quality of the correlation is similar to the one reported by White and Hanusa.²⁰ The scaling method initially reported by Forsyth and Sebag³⁸ and also used by White and Hanusa²⁰ allows to relate calculated chemical shifts to computed shielding constants accordingly to [Equation 1](#).

$$\delta^{\text{calc}} = 0.7463 \sigma^{\text{calc}} + 1973.1 \text{ (Eq. 1)}$$

[Table 3](#) summarizes computed ⁸⁹Y chemical shifts of both neutral and cationic complexes depending on the number of THF molecules bound to the metal center. In parallel, Gibbs energy variations associated to the binding of THF molecules relatives to the non-solvated or least solvated complex and free THF (zero value) are reported as well. Regarding neutral complex **1a**, the ⁸⁹Y chemical shift could be simulated in fair agreement with the experimental value of 879.8 ppm determined in THF-*d*₈ if the metal is coordinated by two THF molecules. This is also in line with the computed binding affinity of THF molecules. Regarding the modeling of complex **1b**, the binding of a THF molecule is computed thermodynamically unfavorable. This most likely result from the loss of an Y..N interaction upon coordination by THF. In terms of NMR calculation, the computed chemical shift of the non-solvated complex is closer to the experimental value but the difference of 75 ppm between computed and experimental shifts remains high. A similar discrepancy is obtained for the modeling of the neutral complex **1c** for which the binding of a THF molecule is computed slightly favorable by 1.4 kcal mol⁻¹. Regarding the cationic complex **2a**, the most stable solvated complex comprises four THF molecules and the two alkyl chains occupy *cis*-positions within the octahedral geometry. For this complex, the difference between computed and experimental ⁸⁹Y chemical shift of 75 ppm is also high.

Table 3. Experimental vs predicted ^{89}Y chemical shifts.

complex	δ^{exp} (solvent) (ppm)	model complex	δ^{calc} (ppm)	$\Delta_r G^{\circ}_{\text{bind}}{}^d$ (kcal mol $^{-1}$)
1a	1109.6 (C $_6$ D $_6$)	Y(CH $_2$ SiMe $_2$ Ph) $_3$	891.7	0.0
	879.5 (THF- d_8)	Y(CH $_2$ SiMe $_2$ Ph) $_3$ (THF)	1012.6	-11.8
		Y(CH $_2$ SiMe $_2$ Ph) $_3$ (THF) $_2$	888.1	-22.6
1b	389.5 (C $_6$ D $_6$)	Y(CH $_2$ C $_6$ H $_4$ NMe $_2$) $_3$	482.6	0.0
	408.5 (THF- d_8)	Y(CH $_2$ C $_6$ H $_4$ NMe $_2$) $_3$ (THF)	492.6	8.2
1c	480.7 (C $_6$ D $_6$)	Y[1,3-(SiMe $_3$) $_2$ C $_3$ H $_3$] $_3$	409.8	0.0
	302.9 (THF- d_8)	Y[1,3-(SiMe $_3$) $_2$ C $_3$ H $_3$] $_3$ (THF)	238.8	-1.4
2a	664.5 (THF- d_8)	[Y(CH $_2$ SiMe $_2$ Ph) $_2$ (THF) $_3$] $^{+,a}$	737.2	0.0
		[Y(CH $_2$ SiMe $_2$ Ph) $_2$ (THF) $_4$] $^{+,b}$	588.9	-7.1
		[Y(CH $_2$ SiMe $_2$ Ph) $_2$ (THF) $_4$] $^{+,c}$	443.0	-1.2
2b	434.4 (THF- d_8)	[Y(CH $_2$ C $_6$ H $_4$ NMe $_2$) $_2$ (THF)] $^+$	372.3	0.0
		[Y(CH $_2$ C $_6$ H $_4$ NMe $_2$) $_2$ (THF) $_2$] $^+$	274.9	-15.9
		[Y(CH $_2$ C $_6$ H $_4$ NMe $_2$) $_2$ (THF) $_3$] $^+$	404.3	-14.9
2c	263.7 (THF- d_8)	[Y[1,3-(SiMe $_3$) $_2$ C $_3$ H $_3$] $_2$ (THF)] $^+$	687.4	0.0
		[Y[1,3-(SiMe $_3$) $_2$ C $_3$ H $_3$] $_2$ (THF) $_2$] $^+$	396.1	-18.8
		[Y[1,3-(SiMe $_3$) $_2$ C $_3$ H $_3$] $_2$ (THF) $_3$] $^+$	439.0	-21.1

a Bipyramid trigonal geometry, alkyls chains in the equatorial plain; b Alkyl chains in *cis*; c Alkyl chains in *trans*; d Difference in Gibbs energy associated to the binding of THF to Y relative the least solvated complex (0.0 value).

A better agreement is obtained concerning the cationic complex **2b** if three THF molecules are bound to the metal center. From this complex the loss of a THF molecule is computed thermo-neutral, suggesting lability of the third THF molecule. Finally, the ^{89}Y chemical shift of the cationic complex **2c** is poorly reproduced even if the metal center binds two or three THF molecules. The difference in Gibbs energy of 2.3 kcal mol $^{-1}$ between these two most stable structures suggests that they are most likely in equilibrium. This peculiarly illustrates the difficulty in computing the

chemical shifts of such complexes in ether solvent, especially cationic ones for which a solvent ligand dynamic exchange is expected in solution.

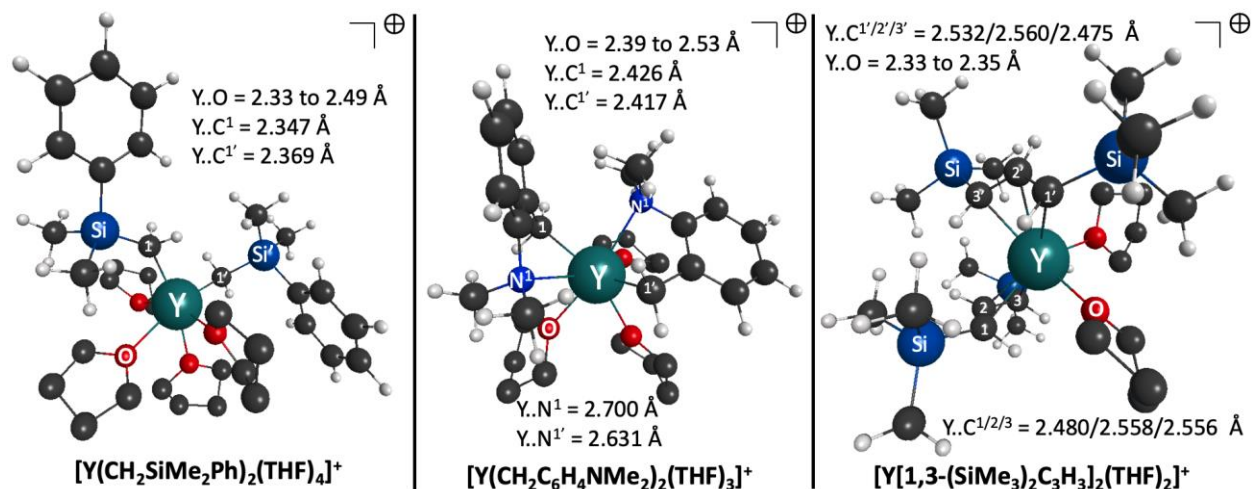


Figure 5. 3D representation of optimized structures of cationic fragments $[Y(CH_2SiMe_2Ph)_2(THF)_4]^+$, $[Y(CH_2C_6H_4NMe_2)_2(THF)_3]^+$, $[Y[1,3-(SiMe_3)_2C_3H_3]_2(THF)_2]^+$, most likely representative of complexes **2a**, **2b** and **2c**, respectively, in THF solution.

As an illustration of the structure of the synthesized cationic complexes, the 3D representation of the optimized structure of cationic fragments $[Y(CH_2SiMe_2Ph)_2(THF)_4]^+$, $[Y(CH_2C_6H_4NMe_2)_2(THF)_3]^+$ and $[Y[1,3-(SiMe_3)_2C_3H_3]_2(THF)_2]^+$ that are respectively and most likely representative of complexes **2a**, **2b** and **2c** in THF solution, is given in Figure 5. In these three cationic complexes, Y..O(THF) distances are ranging from 2.33 to 2.53 Å. For the complex $[Y(CH_2SiMe_2Ph)_2(THF)_4][B(C_6F_5)_4]$ in which the two alkyl groups are *cis*, the Y..C bond distances are ranging from 2.35 to 2.37 Å. Depending on the number of THF molecules coordinated to the metal center, the phenyl ring develops either π -CH weak interaction with a THF ligand, or cation- π interaction with the metal. This highlights the specific role of the $PhSiMe_2-CH_2$

ligand in stabilizing this type of complex. In the *ortho*-toluidinyl complex $[\text{Y}(\text{CH}_2\text{C}_6\text{H}_4\text{NMe}_2)_2(\text{THF})_3][\text{B}(\text{C}_6\text{F}_5)_4]$, Y..N distances of ca. 2.6 Å reflect a strong secondary interaction. In the complex $[\text{Y}[1,3-(\text{SiMe}_3)_2\text{C}_3\text{H}_3]_2(\text{THF})_2][\text{B}(\text{C}_6\text{F}_5)_4]$, both allyl groups remains η^3 -bonded with Y..C bond distances ranging from 2.47 to 2.56 Å. The binding of an additional THF molecules leading to the complex $[\text{Y}[1,3-(\text{SiMe}_3)_2\text{C}_3\text{H}_3]_2(\text{THF})_3][\text{B}(\text{C}_6\text{F}_5)_4]$ induces an η^3 to σ haptotropic shift of one allyl ligand. This induced shift is slightly exergonic by 2.3 kcal mol⁻¹. This reveals the fluxional character of this complex in a THF solution and could account for the difficulty of modelling the NMR signature of the complex and of determining experimentally the number of THF molecules bound to the metal center.

This phenomenon (η^3 - to σ - haptotropic shift of one allyl ligand) can explain the instability of this cationic complex in THF solution (*vide supra*) by transfer of one allyl ligand with the formation of a neutral and dicationic species.

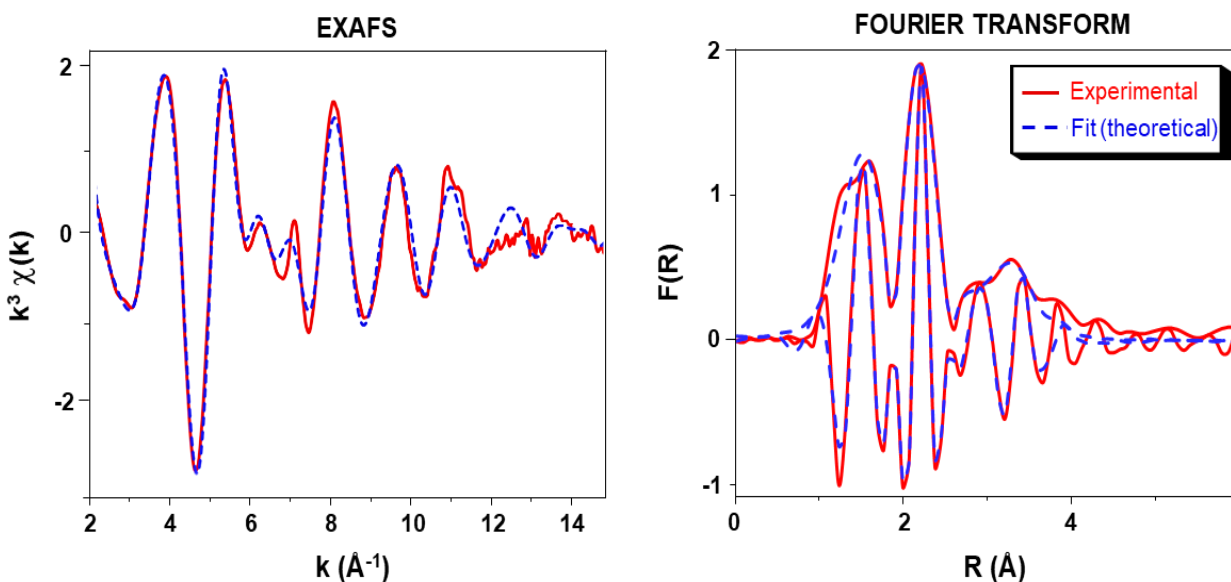


Figure 6. Y K-edge k^3 -weighted EXAFS (left) and Fourier transform (modulus and imaginary part, right) of complex **2c**. Solid lines: Experimental; Dashed lines: Fit using the spherical wave theory.

The cationic molecular complex **2c** with the presumed formula $[\text{Y}[1,3-(\text{SiMe}_3)_2\text{C}_3\text{H}_3]_2(\text{THF})_x][\text{B}(\text{C}_6\text{F}_5)_4]$ was also studied by X-ray absorption spectroscopy (Figure 6) in order to specify its structure and in particular the amount of THF molecules coordinated to Y in the solid state. The fit of the EXAFS signal allowed to precise several structural parameters as indicated in Table 4.

Table 4. EXAFS parameters obtained from the fit of the $k^3 \chi(k)$ signal of the yttrium molecular complex **2c**. The error intervals generated by the fitting program “RoundMidnight” are indicated between parentheses.^a

type of neighbor	number of neighbor	distance Å	σ^2 Å ²
Y-C	6.1(5)	2.57(1)	0.0091(9)
Y--O (THF)	2.1(3)	2.32(2)	0.0091(9) ^b
Y--C (THF)	4.2 ^b	3.18(5)	0.042(17)
Y--Si	4.1 ^b	4.01(3)	0.021(6) ^c

^a Δk : [2.2 - 14.8 Å⁻¹] - ΔR : [0.6 - 4.0 Å]; $S_0^2 = 0.95$; $\Delta E_0 = 4.7 \pm 1.1$ eV (the same for all shells); Fit residue: $\rho = 3.8$ %; Quality factor: $(\Delta\chi)^2/\nu = 2.95$ ($\nu = 17 / 29$); ^bShell constrained to a parameter above. ^cOne type of multiple scattering pathway (Y-C-O, 3 legs) has also been considered in the fit but not mentioned in this table.

The parameters thus extracted from the fit of the $k^3 \chi(k)$ and $k^2 \chi(k)$ EXAFS signals are in agreement with a $[\text{Y}[1,3-(\text{SiMe}_3)_2\text{C}_3\text{H}_3]_2(\text{THF})_2]^+$ structure, with ca. two oxygen atoms at 2.32(2)

Å and ca. six carbon atoms at 2.57(1) Å, as represented in [Figure 5](#). The Y-C distance is close to those observed for $[Y(\eta^5:\eta^1-C_5Me_4SiMe_2NCMe_3)(PMe_3)(\mu-H)]_2$ (2.542(6)-2.729(7) Å) by XRD³⁹ or calculated by DFT for the average Y-C distance in a series of $Y(\eta^3-Me_3SiCHCHCHSiMe_3)_x$ complexes (2.574-2.614 Å).²⁰ The Y-O contribution has been attributed to two THF ligands, though the distance, in the 2.30 - 2.34 Å range, seems a bit short. For instance it is shorter than 2.35(1) Å,⁴⁰ smallest Y--THF bond length observed by XRD for $[Y_3(OCMe_3)_7Cl(THF)_3][BPh_4]$ cationic molecular complex but it is in agreement with the 2.33 - 2.35 Å range found by DFT calculation in this study for the Y-O(THF) distances of **2c** cationic complex in THF solution ([Figure 5](#)). Besides, a contribution of second neighbors greatly improved the fit, with ca. four carbon atoms at 3.18(5) Å, most probably due to two carbon atoms of each THF and ca. four silicon atoms at 4.01(3) Å, which can be attributed to the silicon atoms of the $(\eta^3-Me_3SiCHCHCHSiMe_3)$ allyl ligands. From these results, it can then be concluded that in complex **2c**, two THF molecules seem coordinated to Y, either in the solid state (EXAFS) or in THF solution (DFT calculation).

Catalytic Assays. Ethylene polymerization. Ethylene polymerization experiments were performed at 30 °C in toluene under 5 bars. The polymerization is not initiated if the neutral homoleptic complexes **1a** or **1b** are reacted with the activator $[CPh_3][B(C_6F_5)_4]$ in the presence of 10 equivalents of TiBA ([Table 5](#), runs 1-2). Conversely, cationic complexes **2a-c** are active in ethylene polymerization in the presence of 10 equivalents of $Al(iBu)_3$ (TiBA) ([Table 5](#), runs 3-5). This contrasts, for example, with Y benzamidinate complexes that are catalytic active towards ethylene polymerization upon *in situ* cationization.⁴¹ In absence of TiBA, the cationic catalysts are not active suggesting that TiBA can act as THF scavenger and possibly alkylating agent.

The produced polyethylene by these catalysts has a high dispersity ($\mathcal{D} > 10.8$, Table 5, run 3-5) that results from a bimodal distribution as shown in Figure 7. These two molar mass distributions could result from chain transfer between organo-yttrium cations and tris-alkyl-aluminum via the formation of transient or stable heterobimetallic complexes as reported for example for Nd / Mg based catalytic systems.⁴² In the present case, we can think up the following scenario: (i) chain transfer efficiently takes place between organoyttrium cations and aluminum in the first stage of the polymerization;⁴³ (ii) co-precipitation of insoluble PE chains stored on aluminum; (iii) release of monometallic cationic species that have an enhanced activity till deactivation. In this last stage, high molar mass PE is produced and characterized as the second molar mass distribution.^{42,44}

Table 5. Results of the polymerization of ethylene using complex **1a-b** or **2a-c** in combination with TiBA as co-catalyst and with $[\text{CPh}_3][\text{B}(\text{C}_6\text{F}_5)_4]$ in the case of **1a-b**.

run ^a	complex	mass of polymer yielded (g)	activity ($\text{kg}_{\text{PE}} \text{mol}_{\text{Y}}^{-1} \text{h}^{-1} \text{bar}^{-1}$)	M_n (g mol^{-1}) (\mathcal{D}) ^c
1	1a ^b	0	-	-
2	1b ^b	0	-	-
3	2a	0.50	13.3	5 000 (10.8) ^d
4	2b	0.96	25.6	4 900 (11.8) ^d
5	2c	0.23	6.2	5 300 (13.4) ^d

^aConditions: 60 mL of toluene, 50 °C, 15 μmol of complex, $[\text{Al}] / [\text{Y}] = 10$, $p = 5$ bars, $t = 30$ min.;

^bAddition of 4 mL of a solution containing $[\text{CPh}_3][\text{B}(\text{C}_6\text{F}_5)_4]$ on the solution containing Al and Y compounds at 50 °C under ethylene pressure; ^cDetermined by size exclusion chromatography;

^dBimodal distribution

As *in situ* cationization of the precursor does not initiate polymerization, this set of ethylene polymerization tests demonstrates the interest in isolating cationic species. Additionally, it

provides hints on the catalytically active species. However, since cations **2a**, **2b** and **2c** feature THF molecules in the coordination sphere, TiBA was required as an activator in order to trap THF in order to favor the coordination of the monomer to the metal center during the polymerization.

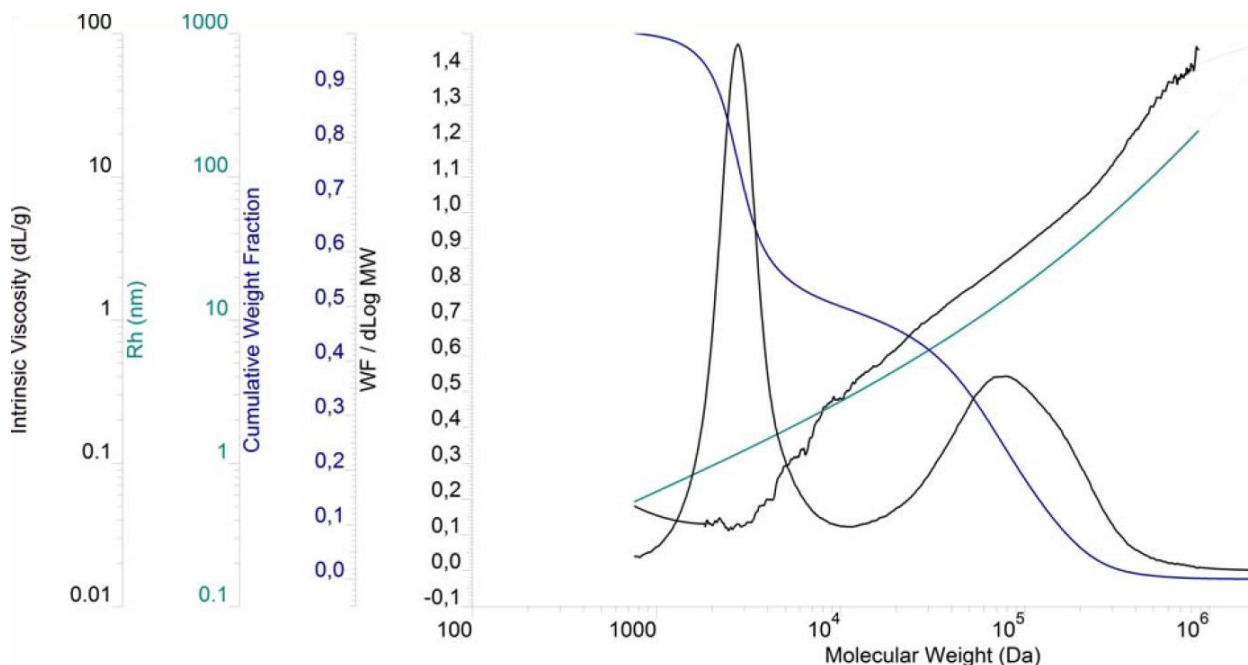
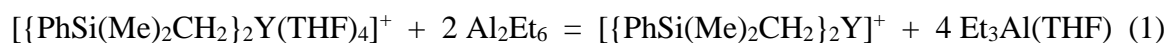


Figure 7. High temperature SEC (150 °C) of polyethylene obtained from **2a**/TiBA (Table 5, run 3).

In order to illustrate this point, the thermodynamics of the following chemical equation has been computed using AlEt₃ as a model of TiBA.



Though the bis-alkyl cation of yttrium $[\{\text{PhSi}(\text{Me})_2\text{CH}_2\}_2\text{Y}]^+$ is poorly stabilized, reaction (1) is computed exergonic by 20.2 kcal mol⁻¹. The driving force of this reaction appears to be the binding of THF molecules to the aluminum dimer Al₂Et₆ to yield Et₃Al(THF) adducts that is computed

exergonic by ca. 32 kcal mol⁻¹. Further reactions of aggregation and transmetalation between $[\{\text{PhSi}(\text{Me})_2\text{CH}_2\}_2\text{Y}]^+$ and Al_2Et_6 have been considered in order to probe dormant and active species. Among all the considered structure, the most stable one is a trimetallic **YAl₂** species in which one $\text{PhSi}(\text{Me})_2\text{CH}_2$ has been displaced by an Et group. In that structure depicted in [Figure 8](#), one AlEt_3 is bridging the Y- $\text{PhSi}(\text{Me})_2\text{CH}_2$ bond and the second AlEt_3 is bridging the Y-Et bond. Additional stability is brought by the Ph ring that is capping the metal center. The loss of this cation- π interaction is unfavorable by ca. 11 kcal mol⁻¹. Attempts to optimize transition state for ethylene insertion either lead to the dissociation of the complex, or to energy barrier that are above 40 kcal mol⁻¹. From **YAl₂**, the release of one AlEt_3 unit lead either top the formation of the bimetallic complex **Y_Al1** or **Y_Al2** ([Figure 8](#)). The formation of these bimetallic complexes is endergonic by 11.0 and 14.9 kcal.mol⁻¹ respectively. Regarding ethylene insertion, the most reactive bond is Y-Et in **YAl_2**. Relative to **YAl2**, the overall Gibbs energy barrier is computed to 24.1 kcal mol⁻¹. In comparison to the $(\text{C}_5\text{Me}_5)_2\text{NdCl}_2\text{Li}(\text{OEt}_2)_2/\text{R}_2\text{Mg}$ ⁴⁵ catalytic system, for which activities are ranging from 200 to 800 kg_{PE} mol_{Nd}⁻¹ h⁻¹ and for which an overall Gibbs energy barrier has been computed 20.6 kcal mol⁻¹, the energy barrier of 24.1 kcal mol⁻¹ computed for the Y/Al system is in fair agreement with activities of ca. 10 kg_{PE} mol_Y⁻¹ h⁻¹.

Interestingly, though not catalytically competent, the structure of $[\{\text{DMPS-CH}_2\}\text{YEt}(\text{AlEt}_3)]^+$ share similarities with Hf/Al cationic heterobimetallic complexes as characterized by NMR and recently reported.⁴⁶ As shown in [Figure 8](#), $[\{\text{DMPS-CH}_2\}\text{YEt}(\text{AlEt}_3)]^+$ displays two β -C-H agostic bonds and a short Y..Al distance of 2.727 Å.

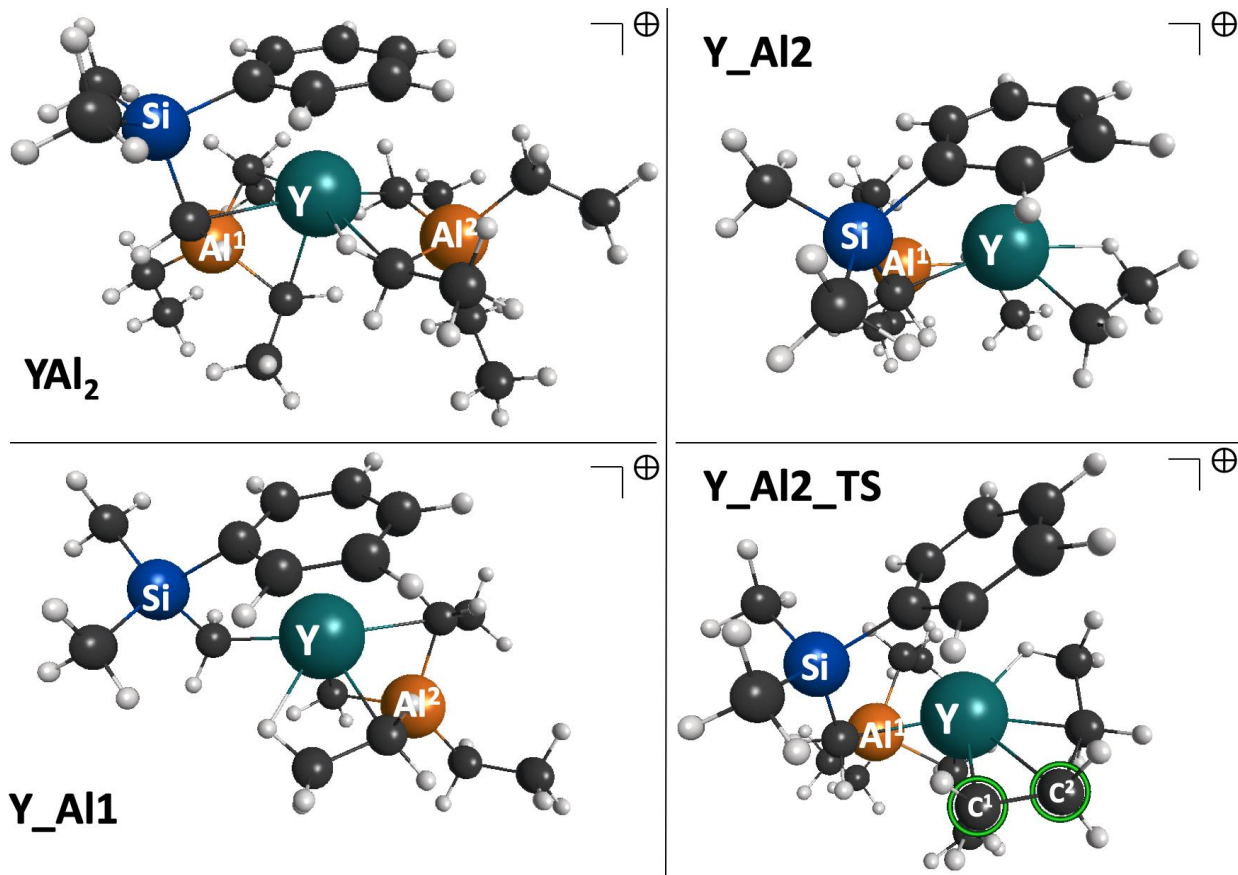


Figure 8. 3D representation of optimized structures of cationic heterobimetallic complexes **YAl₂**, **Y_AI1**, **Y_AI2** and **Y_AI2_TS**.

Isoprene polymerization. Complexes **1a-c** and **2a-c** have been evaluated for isoprene polymerization. In contrast with the ethylene polymerization case, neutral complexes are active for isoprene polymerization upon *in situ* activation by $[\text{CPh}_3][\text{B}(\text{C}_6\text{F}_5)_4]$ and in presence of 10 equivalents of TiBA. The same activation protocol, in which the borate is injected in a mixture of neutral precatalyst, TiBA and monomer, was used for both ethylene and isoprene polymerizations. We can assume that the presence of isoprene and its insertion are required to stabilize the cationic active species formed during the activation step. Note that in absence of alkylaluminum, the combination of **1a-c** with $[\text{CPh}_3][\text{B}(\text{C}_6\text{F}_5)_4]$ does not provide an active species.

Cationic precursors **2a-c** also require TiBA to initiate isoprene polymerization. Under such polymerization condition, the produced polyisoprenes by all the tested and active catalysts show a similar microstructure mainly composed of *cis*-1,4 units (66 to 71 %). The fact that the homoleptic precursors (neutral and cationic) provide similar polyisoprene microstructure, suggests the formation of the same active species in the presence of TiBA. The efficiency of initiation is obtained from the number of chains per yttrium ($n(\text{chains}) = m(\text{PI}) / M_n$). For catalysts obtained with **1a**, **1c**, **2b** and **2c**, approximately one polymer chain grows per yttrium center in agreement with a controlled polymerization. However, only 38% of yttrium initiated a polymer chain for **2a**. In addition, a conversion of 92% are obtained with this complex while full conversion is observed for **2b** and **2c**. These results could be explained by the presence of four THF molecules in the coordination sphere of yttrium. Surprisingly, in the case of the tris(aminobenzyl)yttrium complex **1b**, 2.2 chains are formed per yttrium in agreement with the initiation of two chains per yttrium. The dispersity is ranged from 1.57 to 2.31 suggesting a slow initiation.

In order to better understand the polymerization mechanism, a kinetic studies was carried out with the complex $[\text{Y}(\text{CH}_2\text{C}_6\text{H}_4\text{NMe}_2)_2(\text{THF})_2][\text{B}(\text{C}_6\text{F}_5)_4]$ (**2b**) in presence of TiBA ($[\text{Al}] / [\text{Y}] = 10$) (Table 6, runs 6-10). An increase in molar mass as a function of the conversion is observed as shown in Figure 9. This result agrees with a living character of the polymerization of isoprene. Such a living character has already been characterized for yttrium cationic complexes supporting a bis(phosphinophenyl)amido ligand.⁴⁷

Table 6. Polymerization assays of isoprene using compounds **1a-c** and **2a-c** in combination with TiBA as a co-catalyst, and $[\text{CPh}_3][\text{B}(\text{C}_6\text{F}_5)_4]$ in the case of **1a-b**.

run ^a	complex	time (min)	conversion (%)	M_n^c (g mol ⁻¹) (Đ)	Chains/Y	3,4/ <i>cis</i> -1,4/ <i>trans</i> -1,4 ^d
1	1a ^b	60	90	122 300 (1.9)	1.12	27/66/7
2	1b ^b	60	88	79 000 (1.7)	2.20	25/70/5
3	1c ^b	60	95	160 000 (2.3)	0.86	25/71/4
4	2a	60	92	477 000 (1.6)	0.38	25/71/4
5	2c	60	100	193 000 (1.6)	1.03	27/68/5
6	2b	60	100	173 000 (1.6)	1.16	26/69/5
7	2b	2	6	48 000 (2.3)	0.20	nm
8	2b	5	29	106 000 (1.8)	0.56	27/72/1
9	2b	10	82	132 000 (1.9)	1.25	27/71/2
10	2b	30	97	172 000 (1.9)	1.14	27/70/3

^aConditions: 40 mL toluene, 30 °C, 10 μmol of complex, [isoprene]/[Y] = 3000, [TiBA]/[Y] = 10; ^bAddition of [CPh₃][B(C₆F₅)₄] after precontact of the complex with TiBA ([B]/[Y] = 1); ^cDetermined size exclusion chromatography with triple detection; ^dDetermined from ¹H and ¹³C NMR spectrum of polyisoprene. nm: not measured.

For our system, the dispersity remains high and the molar masses are greater than the theoretical molar mass at the start of polymerization (Figure 9). For a higher conversion, it is noted that the average number molar mass approaches the model with a chain per yttrium. In addition, the number of chains per yttrium stabilizes around 1. Compared to these observations, we believe that the initiation of the polymerization is slow but that the propagation is fast. This would explain the shift from 0.20 to 1.16 chains/Y over time.

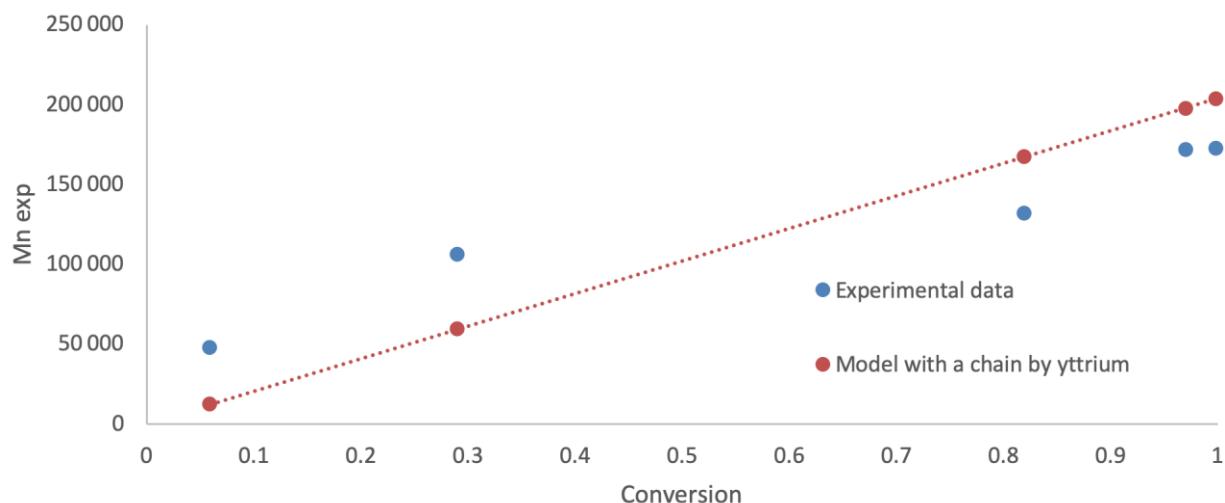


Figure 9. Molar mass curve *vs* conversion for isoprene polymerization catalyzed by **2b** / TiBA (Al / Y = 10) at different times 2, 5, 10, 30 and 60 min; $M_n^{\text{theo}} = 3000 \cdot \text{conversion} \cdot M_{\text{isoprene}} + M_H + M_{\text{isobutyl}}$.

CONCLUSION

In conclusion, new cationic bis-alkyl/allyl yttrium complexes have been synthesized, isolated and fully characterized by different techniques such as elemental analysis, NMR (^1H , ^{13}C , ^{89}Y) and EXAFS for the allyl cationic complex, $[\text{Y}[1,3-(\text{SiMe}_3)_2\text{C}_3\text{H}_3]_2(\text{THF})_2][\text{B}(\text{C}_6\text{F}_5)_4]$. In addition, an original ^{89}Y INEPT sequence has been developed permitting the fast analysis of yttrium complexes by ^{89}Y NMR. In complement, GIAO NMR calculations have been performed at the DFT level in order to corroborate experimental data. Cationic complexes when combined with TiBA are active in polymerization of both ethylene and isoprene. In the latter case, high conversions have been obtained in one hour and the living character of polymerization has been highlighted for catalyst **2b**/TiBA (Al/Y = 10). The microstructure of the yielded polyisoprenes displays mainly *cis*-1,4 units (ca. 60 to 70%) and 3,4 units (ca. 20 to 30%). Only few percent of *trans*-1,4 units are observed.

EXPERIMENTAL SECTION

General procedures

All experiments were performed under a controlled atmosphere by using Schlenk and glovebox techniques for organometallic syntheses. THF (and THF-*d*₈) was purified by distillation from sodium / benzophenone and degassed by freeze pump. Hexane pentane, toluene and C₆D₆ were purified by distillation from NaK and degassed by freeze pump. Reagents: Y(CH₂SiMe₂Ph)₃(THF)₂,²³ Y(CH₂C₆H₄NMe₂)₃,²⁴ and Y[1,3-(SiMe₃)₂C₃H₃]₃,²⁰ were prepared according to published procedures. [PhNMe₂H][B(C₆F₅)₄] from Strem and TiBA from Aldrich was used as received. Isoprene from Aldrich was dried by stirring over CaH₂ for 48 hours and distilled under reduced pressure before use.

Characterization techniques

Elemental analysis. Elemental analyses of the products were performed at the Mikroanalytisches Labor Pascher, Remagen (Germany).

Nuclear Magnetic Resonance analysis. NMR spectra were recorded on Bruker Advance III HD 400 MHz spectrometers in NMR tubes equipped with Teflon (Young) valve. ¹H NMR spectra were referenced to resonances of residual protons of deuterated solvents. ¹³C NMR spectra were referenced to carbon resonances of deuterated solvents and reported in ppm relative to TMS. ⁸⁹Y NMR were externally referenced to 2 M YCl₃ in D₂O. INEPT experiment example: spectra were acquired at 24.51 MHz with a 5 s relaxation delay, with accumulation times of about 30 min (256 scans) in THF-*d*₈ at 293 K. HMBC experiment example: spectra were acquired at 24.51 MHz with pulse prog: hmbcgpndqf in THF-*d*₈ at 293 K. A total of 256 *t*₁ increments were collected. Two transients were averaged for each increment and the recycling delay was 1.5 s. The experiment

was optimized for ${}^2J_{\text{H,Y}} = 2.5$ Hz. Overall experiment time was 15 min. ${}^1\text{H}$ coupled ${}^{89}\text{Y}$ INEPT experiment example: spectra were acquired at 24.51 MHz with a 5 s relaxation delay, with accumulation times of about 1 h (512 number of scan) in C_6D_6 at 293 K.

EXFAS analysis. The cationic bis-allyl yttrium complex **2c** was mixed with dry BN in a mortar within an argon filled glovebox and a pellet of known chemical composition was prepared. This pellet was placed in a double air-tight sample holder equipped with Kapton windows. EXAFS spectra were acquired at ESRF, using BM23 beam-line, at room temperature at the yttrium K-edge (17.04 keV). A pair of Si(111) crystals was used as monochromator and a system based on a total reflection through a double X-ray mirror with an incidence angle variable from 2 to 5 mrad allowed harmonic rejection to better than the 10^{-5} level.⁴⁸ The spectra were recorded in the transmission mode between 16.8 and 18.15 keV. Four scans were collected for the sample. Each data set was collected simultaneously with a Y metal foil reference (17038.4 eV), and was later aligned according to that reference (maximum of the first derivative of the first peak of the Y foil). The data analysis was carried out using the program “Athena”⁴⁹ and the EXAFS fitting program “RoundMidnight”, from the “MAX” package,^{50,51} using spherical waves. The program FEFF8 was used to calculate theoretical files for phases and amplitudes based on model clusters of atoms. The refinements were carried out by fitting the structural parameters N_i , R_i , σ_i and the energy shift, ΔE_0 (the same for all shells) for $k^3 \chi(k)$ and $k^2 \chi(k)$ spectra.

Size Exclusion Chromatography (SEC) analysis. Analyses were performed using a Viscotek system (from Malvern Instruments) equipped with pre-column (PLgel Olexis Guard 7.5x50mm) then three columns (PLgel Olexis Guard 7.5x300mm i.e. from Agilent Technologies). Detector are composed of a refractometer, RALS (Right-Angle Light Scattering), LALS 7° (Low Angle Light Scattering) and viscometer. Portions (100 μL) of sample solutions with concentrations of 3

mg mL⁻¹ were eluted in THF using a flow rate of 1 mL min⁻¹ at 35 °C. The mobile phase was stabilized with 2,6-di-tert-butyl-4-methylphenol (200 mg L⁻¹). The OmniSEC software was used for data acquisition and data analysis. The molar mass distributions were calculated with a calibration curve using a triple calibration.

Syntheses

Synthesis of [Y(CH₂SiMe₂Ph)₂(THF)₄][B(C₆F₅)₄] (2a). A solution of [PhNMe₂H][B(C₆F₅)₄] (234 mg, 0.29 mmol) in 5 mL of THF was added to a solution of Y(CH₂SiMe₂Ph)₃(THF)₂ (200 mg, 0.29 mmol) in 5 mL of THF. The reaction mixture was stirred at room temperature for 30 min. Part of THF was evaporated (3/4 of the volume) and 8 mL of pentane were added. The suspension was cooled for 1h at -30 °C and two phases appeared, the upper phase was discarded, and 8 mL of pentane was added. The mixture was cooled for 1h at -30 °C, the solvent was discarded and the solid/oil yellow was dried under vacuum to give [Y(CH₂SiMe₂Ph)₂(THF)₄][B(C₆F₅)₄] (260 mg, 0.19 mmol, 66% yield). ¹H NMR (400 MHz, THF-*d*₈, 298K): 7.54 ppm (m, 4H, H-Ar), 7.3-7.2 ppm (br, 6H, H-Ar), 3.63 ppm (m, 16H, THF), 1.79 ppm (m, 16H, THF), 0.25 ppm (s, 12H, SiMe), -0.45 ppm (d, J_{Y-CH₂} = 3 Hz, 4H, YCH₂); ¹³C NMR (75.4 MHz, THF-*d*₈, 298K): 143.4 ppm (SiC, Ar), 131.2 ppm (C Ar), 125.7 ppm (C Ar), 125.3 (C Ar), 32.0 ppm (d, J_{YC} = 42 Hz, Y-CH₂), -0.2 ppm (SiMe); ¹⁹F NMR (THF-*d*₈, 298K): -134.6 ppm (br, 2F), -166.8 ppm (t, J = 20 Hz, 1F), -170.4 ppm (t, J = 18 Hz, 2F); ¹¹B NMR (THF-*d*₈, 298K): -16.5 ppm; ⁸⁹Y NMR (19.6 MHz, THF-*d*₈, 298K): 664.5 ppm. Anal. Calcd for C₅₈H₅₈BF₂₀O₄Si₂Y: C, 51.41; H, 4.31; Y, 6.56. Found: C, 50.25; H, 4.19; Y, 7.09.

Note that the resonances of C₆F₅ carbons are too weak to be identified by ¹³C NMR.

Synthesis of [Y(CH₂C₆H₄NMe₂)₂(THF)₂][B(C₆F₅)₄] (2b). A solution of [PhNMe₂H][B(C₆F₅)₄] (326 mg, 0.4 mmol) in 7 mL of THF was added to a solution of Y(CH₂C₆H₄NMe₂)₃ (200 mg, 0.4

mmol) in 4 mL of THF. The reaction mixture was stirred at room temperature for 30 min. Part of THF was evaporated ($\frac{3}{4}$ of the volume) and 8 mL of pentane were added. The suspension was cooled for 1 h at $-30\text{ }^{\circ}\text{C}$ and two phases appear, the upper phase was discarded, and 8 mL of pentane was added. The mixture was cooled for 1 h at $-30\text{ }^{\circ}\text{C}$, the solvent was discarded, and the orange solid / oil was dried under vacuum to give $[\text{Y}(\text{CH}_2\text{C}_6\text{H}_4\text{NMe}_2)_2(\text{THF})_2][\text{B}(\text{C}_6\text{F}_5)_4]$ (318 mg, 0.27 mmol, 68% yield). ^1H NMR (400 MHz, $\text{THF}-d_8$, 298K): 7.42 ppm (d, $J_{\text{HH}} = 8\text{ Hz}$, 2H, H-Ar), 7.16-7.07 ppm (br, 4H, H-Ar), 6.95 (m, 2H, H-Ar), 3.65 ppm (m, 8H, THF), 2.89 ppm (s, 12H, NMe_2), 1.81 ppm (m, 8H, THF), 1.81 and 1.76 ppm (s, 8+4H, THF and YCH_2); ^{13}C NMR (75,4 MHz, $\text{THF}-d_8$, 298K): 140.4 ppm (CN, Ar), 138.1 ppm (C, Ar), , 130.4 ppm (CH, Ar), 128.1 ppm (CH Ar), 121.1 ppm (CH, Ar), 121.0 ppm (CH, Ar), 48.3 ppm (d, $J_{\text{YC}} = 25\text{ Hz}$, YCH_2), 44.3 ppm (NMe_2); ^{19}F RMN ($\text{THF}-d_8$, 298K): -132.8 ppm (br, 2F), -165.0 ppm (t, $J = 20\text{ Hz}$, 1F), -168.5 ppm (t, $J = 18\text{ Hz}$, 2F); ^{11}B NMR ($\text{THF}-d_8$, 328K): -16.5 ppm; ^{89}Y NMR (19.6 MHz, $\text{THF}-d_8$, 328K): 440.4 ppm; Anal. Calcd for $\text{C}_{50}\text{H}_{40}\text{BF}_{20}\text{N}_2\text{O}_2\text{Y}$: C, 50.87; H, 3.42; Y, 7.53. Found C, 50.61; H, 3.44; Y, 7.90.

*Synthesis of $[\text{Y}[1,3-(\text{SiMe}_3)_2\text{C}_3\text{H}_3]_2(\text{THF})_2][\text{B}(\text{C}_6\text{F}_5)_4]$ (**2c**).* A solution of $[\text{PhNMe}_2\text{H}][\text{B}(\text{C}_6\text{F}_5)_4]$ (248 mg, 0.4 mmol) in 5 mL of THF was added to a solution of $\text{Y}[1,3-(\text{SiMe}_3)_2\text{C}_3\text{H}_3]_3$ (200 mg, 0.4 mmol) in 5 mL of THF. The reaction mixture was stirred at room temperature for 30 min. Part of THF was evaporated ($\frac{3}{4}$ of the volume) and 8 mL of pentane were added. The suspension was cooled for 1 h at $-30\text{ }^{\circ}\text{C}$ and two phases appeared, the upper phase was discarded, and 8 mL of pentane was added. The mixture was cooled for 1 h at $-30\text{ }^{\circ}\text{C}$, the solvent was discarded, and the orange solid/oil was dried under vacuum to give $[\text{Y}[1,3-(\text{SiMe}_3)_2\text{C}_3\text{H}_3]_2(\text{THF})_2][\text{B}(\text{C}_6\text{F}_5)_4]$ (**2c**) (204 mg). ^1H NMR (300 MHz, $\text{THF}-d_8$, 298 K): 7.05 ppm (td, $J_{\text{HH}} = 16\text{ Hz}$ and $J_{\text{YH}} = 1.5\text{ Hz}$, 2H, CHCHCH), 3.56 ppm (m, THF), 2.96 ppm (dd, $J_{\text{HH}} = 16\text{ Hz}$

and $J_{YH} = 1.5$ Hz, 4H, *CHCHCH*), 1.81 ppm (m, THF), 0.18 ppm (s, 36H, SiMe₃); ¹H NMR (400 MHz, THF-*d*₈, 298K, 12h after the first analysis): [Y[1,3-(SiMe₃)₂C₃H₃]₂(THF)_n][B(C₆F₅)₄]: 7.05 ppm (td, $J_{HH} = 16$ Hz and $J_{YH} = 1.5$ Hz, 2H, *CHCHCH*), 3.56 ppm (m, THF), 2.96 ppm (dd, $J_{HH} = 16$ Hz and $J_{YH} = 1.5$ Hz, 4H, *CHCHCH*), 1.81 ppm (m, THF), 0.18 ppm (s, 36H, SiMe₃); Y[1,3-(SiMe₃)₂C₃H₃]₃: 7.00 ppm (td, $J_{HH} = 16$ Hz and $J_{YH} = 1.5$ Hz, *CHCHCH*), 3.16 ppm (dd, $J_{HH} = 16$ Hz and $J_{YH} = 1.5$ Hz, *CHCHCH*), 0.14 ppm (s, SiMe₃); ¹³C NMR (75.4 MHz, THF-*d*₈, 298K, 12 h after the first analysis): 163.0 and 160.2 ppm (*CHCHCH* neutral and cationic complexes), 89.8 and 86.4 ppm (d, $J_{YC} = 4$ Hz, *CHCHCH* neutral and cationic complexes), 67.3 ppm (THF), 25.4 ppm (THF), 0.7 and 0.4 ppm (SiMe₃, neutral and cationic complexes); ¹⁹F NMR (THF-*d*₈, 298 K, 12 h after the first analysis): -132.7 ppm (d, $J = 10$ Hz, 2F), -164.9 ppm (t, $J = 20$ Hz, 1F), -168.5 ppm (t, $J = 18$ Hz, 2F); ¹¹B NMR (THF-*d*₈, 298K, 12 h after the first analysis): -16.6 ppm; ⁸⁹Y RMN (19.6 MHz, THF-*d*₈, 298K, 12 h after the first analysis): 263.6 ppm for [Y[1,3-(SiMe₃)₂C₃H₃]₂(THF)₂][B(C₆F₅)₄] and 302.8 ppm for Y[1,3-(SiMe₃)₂C₃H₃]₃.

Typical ethylene polymerization procedure

Cationic precursor (representative example). For ethylene polymerization, an autoclave semi-batch reactor from Top Industry was used. Reactions were carried out in a 200 mL reactor equipped with a mechanical stirrer. In a glove box, the reactor is filled with 57 mL of toluene, then 3 mL of a 50 mM solution of TiBA are added. 23 mg (15 μmol) of the [Y(CH₂SiMe₂Ph)₂(THF)₄][B(C₆F₅)₄] complex (**2a**) are finally added. The reactor is taken out of the glove box and then put under ethylene pressure at 50°C for 30 minutes, overall time of the polymerization reaction. The reactor is allowed to cool down to room temperature, then volume 10 mL methanol is added to stop the reaction. The precipitate is collected and dried by vacuum distillation.

Neutral precursor (representative example). For ethylene polymerization, an autoclave semi-batch reactor from Top Industry was used. Reactions were carried out in a 200 mL reactor equipped with a mechanical stirrer. In a glove box, the reactor is filled with 53 mL of toluene, 0.6 mL of a 50 mM solution of TiBA are added. 2.4 mg (3 μ mol) of the $[Y(CH_2SiMe_2Ph)_3(THF)_2]$ complex (**1a**) are added. In the airlock of the reactor, a solution of 4 mL of toluene containing 3 μ mol of $[CPh_3][B(C_6F_5)_4]$ is added. The reactor is taken out of the glove box and then put under ethylene pressure (3 bars) at 50 °C. Once the temperature is stabilized, the solution of trityl borate is injected under a pressure of 5 bars of ethylene. The solution is stirred for 30 minutes. The reactor is allowed to cool down (to room temperature) and then 10 ml methanol is added to stop the reaction. The precipitate is collected and then dried by vacuum distillation.

Typical isoprene polymerization procedure

Cationic precursor (representative example). In glovebox with argon atmosphere 2 mL of a 50 mM TiBA solution was diluted in 38 mL of toluene, then 2g (30 mmol) of isoprene were added. The solution was stirred overnight. This solution was added to a Schlenk tube containing 15 mg (0.01 mmol) of ion paired complex $[Y(CH_2SiMe_2Ph)_2(THF)_4][B(C_6F_5)_4]$ (**2a**). The mixture was stirred at 30 °C for one hour. After the designated time, the reaction was terminated by adding methanol, and the polymer was precipitated and collected in a large amount of methanol. The polymer was then dried under dynamic vacuum at 70 °C for 3 hours.

Neutral precursor (representative example). In glovebox with argon atmosphere 2 mL of a 50 mM TiBA solution was added in 33 mL of toluene, then 2g (30 mmol) of isoprene were added. The solution was stirred overnight. This solution was transferred to a Schlenk tube containing 7.5 mg (0.01 mmol) of $Y(CH_2SiMe_2Ph)_3(THF)_2$ (**1a**). A solution of 5 mL of toluene is prepared containing 9 mg (0.01 mmol) of trityl borate salt $[CPh_3][B(C_6F_5)_4]$. This solution is poured onto

the solution containing the yttrium complex. The mixture was stirred at 30 °C for one hour. After the designated time, the reaction was terminated by adding methanol, and the polymer was precipitated and collected in a large amount of methanol. The polymer was then dried under dynamic vacuum at 70 °C for 3 hours.

Computational details.

All calculations were performed using the Gaussian 09 D.01 suite of programs.⁵²

Structure and reactivity. Electronic structure calculations were performed at the DFT level using the APFD⁵³ functional. The Stuttgart-Cologne small-core quasi-relativistic pseudopotential ECP28MWB⁵⁴ and its available basis set including up to the g function was used to describe yttrium.⁵⁵ Similarly, silicon and phosphorus were represented by a Stuttgart–Dresden–Bonn pseudopotential⁵⁶ along with the related basis set augmented by a *d* function of polarization ($\alpha_d(\text{P}) = 0.387$; $\alpha_d(\text{Si}) = 0.284$). Other atoms were described by a polarized all electron triple- ζ 6-311G(*d,p*) basis set.³¹ Bulk solvent effect of toluene or THF were simulated using the SMD continuum model.⁵⁷ Transition state optimization was followed by frequency calculations to characterize the stationary point. Intrinsic reaction coordinate (IRC) calculations were performed to confirm the connectivity of the transition states. Gibbs energies were estimated within the harmonic oscillator approximation, and estimated at 298 K and 1 atm.

NMR Calculations. NMR calculations were performed on geometry optimized at the level described above unless specified. Shielding calculations were estimated according to the gauge-including atomic orbitals (GIAO) method^{58,59,60} using the B3LYP^{27,33} functional in conjunction with the 6-311+G(3df,3pd)^{34,35,36} basis set for all atoms except yttrium, which was represented by the triple- ζ basis set of Ahlrich (x2c-TVZPall-2c).³⁷

ASSOCIATED CONTENT

Supporting Information. Supporting energy profiles and additional structural sampling are provided as a supplementary material, as well as all the Cartesian coordinates, associated computed energies and computed NMR shieldings. The following files are available free of charge.

AUTHOR INFORMATION

Corresponding Authors

* e-mail for C.B.: mostafa.taoufik@univ-lyon1.fr

* e-mail for M.T.: christophe.boisson@univ-lyon1.fr

* e-mail for L.P.: lionel.perrin@univ-lyon1.fr

Author Contributions

The manuscript was written through contributions of all authors. All authors have given approval to the final version of the manuscript.

Funding Sources

The authors thank IFP Energies nouvelles and Manufacture Michelin for financial support. L.P thanks the CNRS and le Ministère de l'Enseignement Supérieur et de la Recherche (MESR) for funding.

Notes

The authors declare no competing financial interest.

ACKNOWLEDGMENT

A.E.B. and L.P. thank CCIR facility of ICBMS and P2CHPD computer center of Université Lyon 1 for generous donations of computational time and technical support.

REFERENCES

- (1) Lappert, M. F.; Pearce, R. Stable Silylmethyl and Neopentyl Complexes of Scandium(III) and Yttrium(III). *J. Chem. Soc. Chem. Commun.* **1973**, 126.
- (2) Davidson, P. J.; Lappert, M. F.; Pearce, R. Stable Homoleptic Metal Alkyls. *Acc. Chem. Res.* **1974**, 7, 209–217.
- (3) Zimmermann, M.; Anwander, R. Homoleptic Rare-Earth Metal Complexes Containing Ln–C σ -Bonds. *Chem. Rev.* **2010**, 110, 6194–6259.
- (4) Nakajima, Y.; Okuda, J. Reactivity of Monocationic Bis(Alkyl) and Dicationic Mono(Alkyl) Yttrium Complexes toward Ketones and Carbon Dioxide. *Organometallics* **2007**, 26, 1270–1278.
- (5) Arndt, S.; Okuda, J. Cationic Alkyl Complexes of the Rare-Earth Metals: Synthesis, Structure, and Reactivity. *Adv. Synth. Catal.* **2005**, 347, 339–354.
- (6) Kramer, M. U.; Robert, D.; Nakajima, Y.; Englert, U.; Spaniol, T. P.; Okuda, J. Alkyl Abstraction from a Trialkyl yttrium Complex $[\text{YR}_3(\text{Thf})_2]$ ($\text{R} = \text{CH}_2\text{SiMe}_3$) Using a Group-13 Element Lewis Acid ER_3 ($\text{E} = \text{B}, \text{Al}, \text{Ga}, \text{In}$) – Structural Characterisation of the Ion Pair $[\text{YR}_2(\text{Thf})_4]^+[\text{GaR}_4]^-$ and of ER_3 ($\text{E} = \text{B}, \text{Al}, \text{Ga}$). *Eur. J. Inorg. Chem.* **2007**, 5, 665–674.

(7) Arndt, S.; Zeimentz, P. M.; Spaniol, T. P.; Okuda, J.; Honda, M.; Tatsumi, K. Neutral and Cationic Trimethylsilylmethyl Complexes of the Rare Earth Metals Supported by a Crown Ether: Synthesis and Structural Characterization. *Dalton Trans.* **2003**, *18*, 3622–3627.

(8) Arndt, S.; Spaniol, T. P.; Okuda, J. Homogeneous Ethylene-Polymerization Catalysts Based on Alkyl Cations of the Rare-Earth Metals: Are Dicationic Mono(alkyl) Complexes the Active Species? *Angew. Chem. Int. Ed. Engl.* **2003**, *42*, 5075–5079.

(9) Bambirra, S.; Meetsma, A.; Hessen, B. Lanthanum Tribenzyl Complexes as Convenient Starting Materials for Organolanthanum Chemistry. *Organometallics* **2006**, *25*, 3454–3462.

(10) Schaverien, C. J. Cationic Lanthanide Alkyl Complexes. Evidence for an Unprecedented Tetraphenylborate Coordination Mode in $\text{La}(\text{C}_5\text{Me}_5)\{\text{CH}(\text{SiMe}_3)_2\}\text{BPh}_4$. *Organometallics* **1992**, *11*, 3476–3478.

(11) Bambirra, S.; Bouwkamp, M. W.; Meetsma, A.; Hessen, B. One Ligand Fits All: Cationic Mono(Amidinate) Alkyl Catalysts over the Full Size Range of the Group 3 and Lanthanide Metals. *J. Am. Chem. Soc.* **2004**, *126*, 9182–9183.

(12) Elvidge, B. R.; Arndt, S.; Zeimentz, P. M.; Spaniol, T. P.; Okuda, J. Cationic Rare-Earth Metal Trimethylsilylmethyl Complexes Supported by THF and 12-Crown-4 Ligands: Synthesis and Structural Characterization. *Inorg. Chem.* **2005**, *44*, 6777–6788.

(13) Ge, S.; Bambirra, S.; Meetsma, A.; Hessen, B. The 6-Amino-6-Methyl-1,4-Diazepine Group as an Ancillary Ligand Framework for Neutral and Cationic Scandium and Yttrium Alkyls. *Chem. Commun.* **2006**, *31*, 3320–3322.

(14) Zeimentz, P. M.; Spaniol, T. P.; Okuda, J. Neutral and Cationic Rare-Earth Metal Alkyl Complexes That Contain Bis(2-Methoxyethyl)(Trimethylsilyl)Amine, a Neutral [ONO]-Type Ligand. *Inorganica Chimica Acta* **2006**, *359*, 4769–4773.

(15) Zeimentz, P. M.; Okuda, J. Cationic Aryl Complexes of the Rare-Earth Metals. *Organometallics* **2007**, *26*, 6388–6396.

(16) Fegler, W.; Venugopal, A.; Spaniol, T. P.; Maron, L.; Okuda, J. Reversible Dihydrogen Activation in Cationic Rare-Earth-Metal Polyhydride Complexes. *Angew. Chem. Int. Ed.* **2013**, *52*, 7976–7980.

(17) Li, X.; Nishiura, M.; Hu, L.; Mori, K.; Hou, Z. Alternating and Random Copolymerization of Isoprene and Ethylene Catalyzed by Cationic Half-Sandwich Scandium Alkyls. *J. Am. Chem. Soc.* **2009**, *131*, 13870–13882.

(18) Li, X.; Nishiura, M.; Mori, K.; Mashiko, T.; Hou, Z. Cationic Scandium Aminobenzyl Complexes. Synthesis, Structure and Unprecedented Catalysis of Copolymerization of 1-Hexene and Dicyclopentadiene. *Chem. Commun.* **2007**, *40*, 4137–4139.

(19) Robert, D.; Abinet E.; Spaniol T. P.; Okuda J. Cationic Allyl Complexes of the Rare-Earth Metals: Synthesis, Structural Characterization, and 1,3-Butadiene Polymerization Catalysis. *Chem. Eur.-J.* **2009**, *15*, 11937–11947.

(20) White, R. E.; Hanusa, T. P. Prediction of ^{89}Y NMR Chemical Shifts in Organometallic Complexes with Density Functional Theory. *Organometallics* **2006**, *25*, 5621–5630.

(21) Yu, N.; Nishiura, M.; Li, X.; Xi, Z.; Hou, Z. Cationic Scandium Allyl Complexes Bearing Mono(cyclopentadienyl) Ligands: Synthesis, Novel Structural Variety, and Olefin-Polymerization Catalysis. *Chem. Asian J.* **2008**, *3*, 1406–1414.

(22) Tardif, O.; Kaita, S. Generation of cationic indenyl silylamide gadolinium and scandium complexes $[(\text{Ind})\text{Ln}(\text{N}(\text{SiMe}_3)_2)]^+[\text{B}(\text{C}_6\text{F}_5)_4]^-$ and their reactivity for 1,3-butadiene polymerization. *Dalton Trans.* **2008**, *19*, 2531–2533.

(23) Emslie, D. J. H.; Piers, W. E.; Parvez, M.; McDonald, R. Organometallic Complexes of Scandium and Yttrium Supported by a Bulky Salicylaldimine Ligand. *Organometallics* **2002**, *21*, 4226–4240.

(24) Zhang, W.-X.; Nishiura, M.; Mashiko, T.; Hou, Z. Half-Sandwich *o*-N,N-Dimethylaminobenzyl Complexes over the Full Size Range of Group 3 and Lanthanide Metals. Synthesis, Structural Characterization, and Catalysis of Phosphine P-H Bond Addition to Carbodiimides. *Chem. Eur. J.* **2008**, *14*, 2167–2179.

(25) Jameson, C. J. Understanding NMR Chemical Shifts. *Annu. Rev. Phys. Chem.* **1996**, *47*, 135–169.

(26) Ylihautala, M.; Lounila, J.; Jokisaari, J. Nuclear magnetic shielding of noble gases in liquid crystals. *J. Chem. Phys.* **1999**, *110*, 6381–6388.

(27) Becke, A. D. Density-functional thermochemistry. III. The role of exact exchange. *J. Chem. Phys.* **1993**, *98*, 5648–5652.

(28) Perdew, J. P.; Wang, Y. Accurate and simple analytic representation of the electron-gas correlation energy. *Phys. Rev. B* **1992**, *45*, 13244–13249.

(29) Schaverien, C. J. Alkoxides as ancillary ligands in organolanthanide chemistry: synthesis of, reactivity of, and olefin polymerization by the μ -hydride- μ -alkyl compounds $[\text{Y}(\text{C}_5\text{Me}_5)(\text{OC}_6\text{H}_3\text{tBu}_2)]_2(\mu\text{-H})(\mu\text{-alkyl})$. *Organometallics* **1994**, *13*, 69–82.

(30) Evans, W. J.; Peterson, T. T.; Rausch, M. D.; Hunter, W. E.; Zhang, H.; Atwood, J. L. Synthesis and x-ray crystallographic characterization of an asymmetric organoyttrium halide dimer: $(\text{C}_5\text{Me}_5)_2\text{Y}(\mu\text{-Cl})\text{YCl}(\text{C}_5\text{Me}_5)_2$. *Organometallics* **1985**, *4*, 554–559.

(31) McLean, A. D.; Chandler, G. S. Contracted Gaussian-basis sets for molecular calculations. 1. 2nd row atoms, $Z=11-18$. *J. Chem. Phys.* **1980**, *72*, 5639–5648; Raghavachari, K.; Binkley, J. S.; Seeger, R.; Pople, J. A. Self-Consistent Molecular Orbital Methods. 20. Basis set for correlated wave-functions. *J. Chem. Phys.* **1980**, *72*, 650–654.

(32) Godbout, N.; Salahub, D. R.; Andzelm, J.; Wimmer, E. Optimization of Gaussian-type basis sets for local spin density functional calculations. Part I. Boron through neon, optimization technique and validation. *Can. J. Chem.* **1992**, *70*, 560–571.

(33) Lee, C.; Yang, W.; Parr, R.G. Development of the Colle-Salvetti correlation-energy formula into a functional of the electron density. *Phys. Rev. B* **1988**, *37*, 785–789.

(34) Clark, T.; Chandrasekhar, J.; Spitznagel, G. W.; Schleyer, P. V. R. Efficient diffuse function-augmented basis sets for anion calculations. III. The 3-21+G basis set for first-row elements, Li-F. *J. Comput. Chem.* **1983**, *4*, 294–301.

(35) Frisch, M. J.; Pople, J. A.; Binkley, J. S. Self-consistent molecular orbital methods 25. Supplementary functions for Gaussian basis sets. *J. Chem. Phys.* **1984**, *80*, 3265–3269.

(36) Krishnan, R.; Binkley, J. S.; Seeger, R.; Pople, J. A. Self-consistent molecular orbital methods. XX. A basis set for correlated wave functions. *J. Chem. Phys.* **1980**, *72*, 650–654.

(37) Pollak, P.; Weigend, F. Segmented Contracted Error-Consistent Basis Sets of Double- and Triple- ζ Valence Quality for One- and Two-Component Relativistic All-Electron Calculations. *J. Chem. Theory Comput.* **2017**, *13*, 3696–3705.

(38) Forsyth, D. A.; Sebag, A. B. Computed ^{13}C NMR Chemical Shifts via Empirically Scaled GIAO Shieldings and Molecular Mechanics Geometries. Conformation and Configuration from ^{13}C Shifts. *J. Am. Chem. Soc.* **1997**, *119*, 40, 9483–9494.

(39) Arndt, S.; Voth, P.; Spaniol, T. P.; Okuda J. Dimeric Hydrido Complexes of Rare-Earth Metals Containing a Linked Amido-Cyclopentadienyl Ligand: Synthesis, Characterization and Monomer-Dimer Equilibrium. *Organometallics* **2000**, *19*, 4690–4700.

(40) Evans, W. J.; Olofson, J. M.; Ziller, J. W. Synthesis and Structure of the Cationic tert-Butoxide Complexes $\text{Y}_3(\text{OR})_7\text{Cl}(\text{THF})^{3+}$, $\text{Y}_2(\text{OR})_4\text{Cl}(\text{THF})_4^+$, and $\text{Y}(\text{OR})\text{Cl}(\text{THF})_5^+$: Representatives of a New Class of Yttrium Alkoxides. *J. Am. Chem. Soc.* **1990**, *112*, 2308–2314.

(41) S. Bambirra, D. van Leusen, A. Meetsma, B. Hessen and J. H. Teuben, *Chem. Commun.* **2003**, 522–523.

(42) Nsiri, H.; Belaid, I.; Larini, P.; Thuilliez, J.; Boisson, C.; Perrin, L. Ethylene-Butadiene Copolymerization by Neodymocene Complexes: A Ligand Structure / Activity / Polymer Microstructure Relationship Based on DFT Calculations. *ACS Catal.* **2016**, *6*, 1028–1036.

(43) Valente, A.; Mortreux, A.; Visseaux, M.; Zinck, P. Coordinative Chain Transfer Polymerization. *Chem. Rev.* **2013**, *113*, 3836–3857.

(44) Boisson, C.; Monteil, V.; Ribour, D.; Spitz, R.; Barbotin, F. *Macromol. Chem. Phys.* **2003**, *204*, 1747–1754.

(45) Ribeiro, R.; Ruivo, R.; Nsiri, H.; Norsic, S.; D'Agosto, F.; Perrin, L.; Boisson, C. Deciphering the mechanism of Coordinative Chain Transfer Polymerization of ethylene using neodymocene catalysts and dialkylmagnesium. *ACS Catal.* **2016**, *6*, 851–860.

(46) Tensi, L.; Froese, R. D. J.; Kuhlman, R. L.; Macchioni, A.; Zuccaccia, C. Interception of Elusive Cationic Hf–Al and Hf–Zn Heterobimetallic Adducts with Mixed Alkyl Bridges Featuring Multiple Agostic Interactions. *Chem. Eur.-J.* **2020**, *26*, 3758–3766.

(47) Zhang, L.; Suzuki, T.; Luo, Y.; Nishiura, M.; Hou, Z. Cationic Alkyl Rare-Earth Metal Complexes Bearing an Ancillary Bis(Phosphinophenyl)Amido Ligand: A Catalytic System for Living Cis-1,4-Polymerization and Copolymerization of Isoprene and Butadiene. *Angew. Chem. Int. Ed.* **2007**, *46*, 1909–1913.

(48) Mathon, O.; Beteva, A.; Borrel, J.; Bugnazet, D.; Gatla, S.; Hino, R.; Kantor, I.; Mairs, T.; Munoz, M.; Pasternak, S.; Perrin, F.; Pascarelli, S. The time-resolved and extreme conditions XAS (TEXAS) facility at the European Synchrotron Radiation Facility: the general-purpose EXAFS bending-magnet beamline BM23. *J. Synchrotron Rad.* **2015**, *22*, 1548–1554.

(49) Ravel, B.; Newville, M. Athena, Artemis, Hephaestus: data analysis for X-ray absorption spectroscopy using IFEFFIT. *J. Synchrotron Rad.* **2005**, *12*, 537–541.

(50) Michalowicz, A.; Moscovici, J.; Muller-Bouvet, D.; Provost, K. MAX: Multiplatform Applications for XAFS. *J. Phys. Conf. Ser.* **2009**, *190*, 012034.

(51) Michalowicz, A. EXAFS pour le MAC, in *Logiciels pour la Chimie*, (Ed. Société Française de Chimie, Paris,) 1991, 102–103.

(52) Gaussian 09, Revision D.01, Frisch, M. J.; Trucks, G. W.; Schlegel, H. B.; Scuseria, G. E.; Robb, M. A.; Cheeseman, J. R.; Scalmani, G.; Barone, V.; Mennucci, B.; Petersson, G. A.; Nakatsuji, H.; Caricato, M.; Li, X.; Hratchian, H. P.; Izmaylov, A. F.; Bloino, J.; Zheng, G.; Sonnenberg, J. L.; Hada, M.; Ehara, M.; Toyota, K.; Fukuda, R.; Hasegawa, J.; Ishida, M.; Nakajima, T.; Honda, Y.; Kitao, O.; Nakai, H.; Vreven, T.; Montgomery Jr., J. A.; Peralta, J. E.; Ogliaro, F.; Bearpark, M.; Heyd, J. J.; Brothers, E.; Kudin, K. N.; Staroverov, V. N.; Kobayashi, R.; Normand, J.; Raghavachari, K.; Rendell, A.; Burant, J. C.; Iyengar, S. S.; Tomasi, J.; Cossi, M.; Rega, N.; Millam, J. M.; Klene, M.; Knox, J. E.; Cross, J. B.; Bakken, V.; Adamo, C.; Jaramillo, J.; Gomperts, R.; Stratmann, R. E.; Yazyev, O.; Austin, A. J.; Cammi, R.; Pomelli, C.; Ochterski, J. W.; Martin, R. L.; Morokuma, K.; Zakrzewski, V. G.; Voth, G. A.; Salvador, P.; Dannenberg, J. J.; Dapprich, S.; Daniels, A. D.; Farkas, Ö.; Foresman, J. B.; Ortiz, J. V.; Cioslowski, J.; Fox, D. J. Gaussian, Inc., Wallingford CT, 2009.

(53) Austin, A.; Petersson, G.; Frisch, M. J.; Dobek, F. J.; Scalmani, G.; Throssell, K. A density functional with spherical atom dispersion terms. *J. Chem. Theory and Comput.* **2012**, *8*, 4989–5007.

(54) Andrae, D.; Häußermann, U.; Dolg, M.; Stoll H.; Preuss H. Energy-adjusted ab initio pseudopotentials for the second and third row transition elements. *Theor. Chim. Acta* **1990**, *77*, 123–141.

(55) Martin, J. M. L.; Sundermann, A. Correlation consistent valence basis sets for use with the Stuttgart–Dresden–Bonn relativistic effective core potentials: The atoms Ga–Kr and In–Xe. *J. Chem. Phys.* **2001**, *114*, 3408.

(56) Bergner, A.; Dolg, M.; Kuechle, W.; Stoll, H.; Preuss, H. Ab initio energy-adjusted pseudopotentials for elements of groups 13–17. *Mol. Phys.* **1993**, *80*, 1431–1441.

(57) Marenich, A. V.; Cramer, C. J.; Truhlar, D. G. Universal solvation model based on solute electron density and a continuum model of the solvent defined by the bulk dielectric constant and atomic surface tensions. *J. Phys. Chem. B* **2009**, *113*, 6378–6396.

(58) Ditchfield, R. Self-consistent perturbation theory of diamagnetism. 1. Gauge-invariant LCAO method for N.M.R. chemical shifts. *Mol. Phys.* **1974**, *27*, 789–807.

(59) Wolinski, K.; Hilton, J. F.; Pulay, P. Efficient Implementation of the Gauge-Independent Atomic Orbital Method for NMR Chemical Shift Calculations. *J. Am. Chem. Soc.* **1990**, *112*, 8251–8260.

(60) Cheeseman, J. R.; Trucks, G. W.; Keith, T. A.; Frisch, M. J. A Comparison of Models for Calculating Nuclear Magnetic Resonance Shielding Tensors. *J. Chem. Phys.* **1996**, *104*, 5497–5509.

GRAPHICAL TOC

